



## RESEARCH ARTICLE

10.1029/2021JD035260

### Key Points:

- The numerical model employed is able to simulate the main steady state saltation characteristics
- Cohesion and grain size heterogeneity increase snow saltation mass flux at high friction velocities
- Improved estimates of snow saltation mass flux and concentration must take into account the bed properties

### Correspondence to:

D. B. Melo,  
daniela.britomelo@epfl.ch

### Citation:

Melo, D. B., Sharma, V., Comola, F., Sigmund, A., & Lehning, M. (2022). Modeling snow saltation: The effect of grain size and interparticle cohesion. *Journal of Geophysical Research: Atmospheres*, 127, e2021JD035260. <https://doi.org/10.1029/2021JD035260>

Received 12 MAY 2021

Accepted 3 DEC 2021

## Modeling Snow Saltation: The Effect of Grain Size and Interparticle Cohesion

**D. B. Melo<sup>1</sup> , V. Sharma<sup>1</sup>, F. Comola<sup>2</sup> , A. Sigmund<sup>1</sup> , and M. Lehning<sup>1,3</sup>**

<sup>1</sup>School of Architecture, Civil and Environmental Engineering, Ecole Polytechnique Fédérale de Lausanne, Lausanne, Switzerland, <sup>2</sup>Department of Atmospheric and Oceanic Sciences, University of California, Los Angeles, Los Angeles, CA, USA, <sup>3</sup>WSL Institute of Snow and Avalanche Research SLF, Davos, Switzerland

**Abstract** The surface of the Earth is snow-covered at least seasonally over large areas. This snow surface is highly dynamic, particularly under the influence of strong winds. The motion of snow particles driven by the wind not only changes the snow cover but has important consequences for the atmosphere in that it adds mass and moisture and extracts heat. Large scale meteorological and climatological models neglect these surface dynamics or produce conflicting results from too simplified process representation. With recent progress in the detailed understanding of the saltation process, in particular with respect to sand saltation, and the advancement of numerical models, we can systematically investigate the influence of snow properties on saltation. This contribution uses a Large Eddy Simulation model with full surface particle dynamics to investigate how snow cohesion and size distribution influence saltation dynamics and in particular the total mass flux. The model reproduces some known characteristics of the saltation system such as a focus point or a constant near surface particle speed. An interesting result is that cohesion and grain size heterogeneity can increase the overall saltation mass flux at high friction velocities. Moreover, some simplified models agree reasonably well with the simulations for given bed characteristics, while others clearly do not. These results are valid for continuous saltation while intermittent saltation, which often occurs in nature, needs further investigation. In order to successfully parameterize saltation in large scale models, progress must be made in correctly representing snow surface properties in these models, in particular cohesion.

### 1. Introduction

Wind erosion of snow covered surfaces is frequently observed in alpine and polar regions. Snow transport leads to the formation of bedforms, intensifies snow sublimation and modifies the microstructure of surface snow layers. Moreover, the interaction between the wind field and the complex topography creates regions of enhanced snow erosion and deposition, which greatly contributes to snow height heterogeneity. In alpine regions, these processes are of great importance for water management and avalanche risk assessment (Lehning et al., 2008). In Antarctica, snow transport is enhanced by the katabatic winds, dominating large areas from the inner plateau to the coast, and clouds of blowing snow particles with a height of hundreds of meters can be observed (Palm et al., 2017).

The aeolian transport of snow occurs at different heights above the ground. The terms drifting snow and blowing snow are commonly used to indicate, respectively, the movement of snow particles close to the surface (up to ~2 m height) and the movement of smaller snow particles transported at high elevations. Three transport modes (creep, saltation and suspension) are commonly distinguished during snow transport events (Bagnold, 1941). The rolling and sliding of snow grains along the surface is defined as creep. Creeping particles are typically too large and heavy to be lifted by the flow. During drifting snow events, their motion is mainly driven by impacting particles. Saltation refers to the ballistic motion of particles close to the ground. Particles in saltation generally hit the ground with enough kinetic energy to hop again (rebound) or eject other particles on the bed (splash). They are mostly concentrated in the first 10 cm above the surface and the ensemble of saltating particles constitute the saltation layer. Suspension refers to the motion of smaller snow particles transported above the saltation layer. They mainly follow the wind flow and travel great distances before being deposited on the ground or sublimate.

At low wind speeds, the mass flux in saltation is greater than the mass flux of suspended particles (Gordon et al., 2009; Nishimura & Nemoto, 2005). At high wind speeds, snow transport in suspension becomes relevant and is currently simulated in mesoscale models by advection-diffusion equations (Amory et al., 2015, 2021; Déry & Yau, 1999; Lehning et al., 2008; Lenaerts et al., 2012; Vionnet et al., 2014). Particle concentration in the

© 2021. The Authors.

This is an open access article under the terms of the [Creative Commons Attribution License](#), which permits use, distribution and reproduction in any medium, provided the original work is properly cited.

saltation layer defines the lower boundary condition for snow suspension. The saltation models commonly used in these mesoscale models rely on simple analytical equations based on the assumption of steady state saltation, that is, an equilibrium state between the grains in motion and the wind field (Doorschot & Lehning, 2002; Pomeroy & Gray, 1990; Sørensen, 2004). However, the parameters used in the referred analytical saltation models are highly uncertain and do not always reflect the properties of the snow type. This limits the accuracy of the mass flux of particles in suspension, which is usually underestimated (Amory et al., 2015) or overestimated (Vionnet et al., 2014, 2017). As a consequence, uncertainties arise in the rate of blowing snow sublimation and the consequent increase in the atmospheric moisture content. For instance, snow sublimation is the main mass-depleting process in some regions of the Antarctic ice sheet, but the contribution of blowing snow sublimation is still largely unknown (Agosta et al., 2019; Van Wessem et al., 2018). Hence, even though snow saltation is usually a sub-grid process in mesoscale models, its correct modeling greatly influences the mass and energy balances at a larger scale.

The complexity of modeling snow saltation is related to the turbulent flow features and the snow particle characteristics. In contrast with sand beds, snow beds change continuously: soon after deposition, snow grains form interparticle ice bonds between each other; the characteristics of a snow bed (for instance, particle size distribution, interparticle bonds and grain shape) evolve with time due to metamorphic processes; and snow particle size and shape change during saltation events due to fragmentation (Comola et al., 2017) and sublimation (Sharma et al., 2018).

Detailed models of saltation are ideal to simulate both the flow and snow bed particularities. By explicitly solving the turbulent flow, particle trajectories and the surface processes, these models can be used to improve our understanding of particle-wind interaction and to evaluate some of the assumptions made in simple saltation models. In the last two decades, Reynolds-Averaged Navier-Stokes (RANS) and Large Eddy Simulation (LES) flow solver techniques were used, coupled with Lagrangian models for particle dynamics (e.g., Almeida et al., 2006; Dupont et al., 2013; Groot Zwaftink et al., 2014; Okaze et al., 2018; Shao & Li, 1999). Moreover, splash laws based on conservation principles were also proposed and used to describe steady state saltation (Comola & Lehning, 2017; Kok & Renno, 2009; Lämmel et al., 2017).

Sophisticated measurement techniques based on imaging and particle tracking algorithms have provided detailed observations of near-surface particle motion and an insight on the role played by high-frequency wind turbulence on snow saltation dynamics (e.g., Aksamit & Pomeroy, 2016, 2018; Gromke et al., 2014; Paterna et al., 2016, 2017). In particular, Paterna et al. (2016) have shown some evidence that velocity fluctuations significantly influence the vertical mass flux of saltating snow. Aksamit and Pomeroy (2018) have observed that both low- and high-frequency turbulence structures impact drifting snow dynamics. These findings strongly support the need for an accurate description of the turbulent flow field when modeling the wind-particle interaction intrinsic to snow saltation.

Recent theoretical and numerical advances (Comola, Gaume, et al., 2019; Comola & Lehning, 2017) have shed light into the role played by granular bed properties, such as grain size distribution and interparticle cohesion, in granular splash mechanisms. In addition, field measurements of drifting snow in alpine terrain (Aksamit & Pomeroy, 2016) have shown that snow surface hardness influences the mean vertical profiles of particle velocity and mass flux during intermittent saltation. However, the effect of snow surface properties on saltation development and scaling laws is still largely unknown. For example, there are no quantitative estimates on how particle size distribution and interparticle cohesion influence particle speed and surface friction velocity during saltation. Consequently, the effect of surface properties on the integrated mass flux is still unclear.

In this work, we use an LES solver coupled with a Lagrangian model to compute particle-wind interactions (Comola, 2017) and the splash functions proposed by Comola and Lehning (2017) to describe particle-bed interactions. The capabilities of this model to simulate steady state saltation are firstly assessed. The vertical profiles of wind speed, saltation mass flux, concentration and particle velocity are analyzed, as well as the variation of the integrated mass flux with the friction velocity. Then, a detailed study on the effect of grain size and interparticle cohesion on the vertical profiles, integrated mass flux and surface friction velocity is performed. To this end, the properties of the granular bed are varied in a systematic way in a suite of simulations, which cover a range of wind velocities. The results are compared to existing saltation models and to the conclusions drawn from the latest wind tunnel and field experiments.

This article shows the potential of LES-based models coupled with state-of-the-art splash functions to simulate steady state saltation and to improve our understanding of saltation dynamics. Moreover, it sheds light onto the relative importance of grain size and interparticle cohesion for snow saltation characteristics. The work presented ultimately helps progressing toward the development of new saltation mass flux parameterizations, which would take into account the influence of surface snow properties.

The model details are presented in Section 2. In Section 3, the numerical setup used for the simulations is presented. The results are shown and discussed in Section 4 and the main conclusions are summarized in Section 5.

## 2. Flow and Particle Dynamics

### 2.1. Flow Solver

The tri-dimensional wind field is solved with the Large Eddy Simulation (LES) technique. Turbulence features larger than the grid size are resolved by the filtered continuity and Navier-Stokes equations, while the effect of smaller eddies is parameterized by a sub-grid scale (SGS) model. The LES model used along with the particles solver is named EPFL-LES. It was developed at the Ecole Polytechnique Fédérale de Lausanne and is based on the work of Albertson and Parlange (1999).

The LES code targets atmospheric boundary layer (ABL) flows, assumed incompressible and driven by a constant streamwise pressure gradient,  $\partial p_\infty / \partial x$  [Pa m<sup>-1</sup>]:

$$\frac{\partial p_\infty}{\partial x} = -\rho_f \frac{u_*^2}{L_z} \quad (1)$$

where  $\rho_f$  [kg m<sup>-3</sup>] is the fluid density,  $L_z$  [m] is the domain height and  $u_*$  [m s<sup>-1</sup>] is the desired friction velocity.

Horizontal gradients are computed with a Fourier-based pseudo-spectral approach and vertical gradients are calculated using second-order finite differences. The time derivatives are computed with the second-order Adams-Bashforth time advancement scheme (Canuto et al., 1988). In the present code version, the closure SGS model is given by the scale-dependent Lagrangian dynamic model (LASD) as proposed by Bou-Zeid et al. (2005). This model exhibits better dissipation characteristics than the classic Smagorinsky and the scale-invariant dynamic models.

Periodic boundary conditions are imposed in the vertical walls of the computational domain, as required when applying Fourier transforms, allowing for the development of a fully turbulent flow at both the inlet and outlet sections. At the top boundary, impermeability and zero vertical gradients are assumed. At the bottom boundary, the impermeability condition is imposed and the wall shear stress is given by the logarithmic law of the wall. The use of wall functions avoids highly discretized meshes near the surface as well as smaller time steps to guarantee numerical stability.

The present LES code has been used in multiple ABL studies concerning land-atmosphere interaction over complex terrains, wind-farms and urban canopy (Albertson & Parlange, 1999; Bou-Zeid et al., 2005; Diebold et al., 2013; Giometto et al., 2016, 2017; Sharma et al., 2017). A detailed description of the model can be found in these works.

### 2.2. Particle Dynamics

Particle motion is computed in a Lagrangian framework. The coupling with the LES solver was developed by Comola (2017), following the work of Groot Zwaftink et al. (2014). The model has been further developed with the contributions of Comola and Lehning (2017), Sharma et al. (2018) and Comola, Giometto, et al. (2019).

Particle inertia, gravity and aerodynamic drag are related by Newton's second law. Aerodynamic drag,  $D_i$  [N], is given by  $D_i = -1/2C_D\rho_f A_f |U_r| U_{r,i}$ , where  $i = 1, 2, 3$  denotes the  $x$  [m] (streamwise),  $y$  [m] (crosswise) and  $z$  [m] (vertical) directions in the Cartesian coordinate system.  $C_D$  is the drag coefficient,  $A_f$  [m<sup>2</sup>] is the particle frontal area,  $U_{r,i}$  [m s<sup>-1</sup>] the particle velocity relative to the local flow and  $|U_r|$  [m s<sup>-1</sup>] its absolute value (henceforth referred to as  $U_r$ ). In the current model, saltating particles are assumed spherical, with a frontal area  $A_f = \pi d^2/4$ , where  $d$  [m] is the particle diameter. The drag coefficient is estimated using the expression proposed

by Schiller and Nauman (1933). It is a function of the particle Reynolds number,  $Re_d = U_r d / \nu_f$ , where  $\nu_f$  [ $m^2 s^{-1}$ ] is the fluid kinematic viscosity:

$$C_D = \frac{24}{Re_d} (1 + 0.15 Re_d^{0.687}). \quad (2)$$

This expression was obtained from fitting experimental measurements developed with spherical particles of multiple sizes and is valid for  $Re_d < 800$ . Hence, it describes both the Stokes and transition flow regimes, which are characteristic of aeolian saltation.

The assumption of spherical particles is widely used in saltation models (e.g., Doorschot & Lehning, 2002; Nemoto & Nishimura, 2004; Schmidt, 1980) and in optical measurements of snow size distribution and mass flux (e.g., Crivelli et al., 2016; Guala et al., 2008). Even though snowfall particles can have multiple shapes according to the meteorological conditions upon formation, particles in saltation exhibit a different shape and size distribution than falling snow: they are generally smaller, denser and more rounded (Nishimura & Nemoto, 2005; Walden et al., 2003; Woods et al., 2008) due to particle fragmentation after multiple impacts with the bed (Comola et al., 2017). In fact, a layer of wind packed snow composed of small and closely packed grains is commonly observed after drifting snow events (Fierz et al., 2009). These observations support the assumption of spherical particles when modeling the wind-particle interaction in steady state saltation. However, the drag law could be improved to take into account the effect of surface irregularities (Kok & Renno, 2009). According to the studies of Dietrich (1982) developed with sand particles, geometrical deviations from a spherical shape can encompass high curvature regions that promote flow separation. Therefore, the drag coefficient is expected to be slightly higher for non-spherical particles. In addition, different drag laws could be employed to better represent fresh snow at saltation onset or when drifting snow occurs with concurrent snowfall, as proposed by Tagliavini et al. (2021) for falling snow crystals.

The equation for particle trajectory yields:

$$du_{p,i} = \left[ \frac{3}{4} \frac{\rho_f}{\rho_p} \frac{C_D}{d} U_r (u_i - u_{p,i}) - g \delta_{i3} \right] dt \quad (3)$$

where  $u_{p,i}$  [ $m s^{-1}$ ] is the particle velocity,  $u_i$  [ $m s^{-1}$ ] is the instantaneous flow velocity resolved by the LES solver,  $\rho_p$  [ $kg m^{-3}$ ] is the particle density,  $g$  [ $m s^{-2}$ ] is the acceleration of gravity,  $t$  [s] is the time variable and  $\delta$  is the Kronecker delta. Equation 3 is solved numerically with a first-order forward Euler method.

Other forces such as aerodynamic lift, electrostatic forces and those from interparticle collision are expected to be smaller than weight and drag and are generally neglected when modeling saltation in air (Anderson & Hallet, 1986; Maxey & Riley, 1983). Their effect on sand saltation was studied by several authors (e.g., Durán et al., 2011; Huang et al., 2007; Kok & Renno, 2006, 2008; Schmidt et al., 1998) and further investigation is needed to fully assess their impact on particle trajectory (Kok et al., 2012).

In previous works based on this model (Comola, Giometto, et al., 2019; Groot Zwaftink et al., 2014; Sharma et al., 2018), the non-resolved SGS velocities were computed. Then, the instantaneous wind field was derived from the sum of the resolved wind velocity field,  $u_i$ , and the SGS velocities. The modeling of velocity fluctuations is important when using simple flow models, as COMSALT (Kok & Renno, 2009), or RANS solvers (Nemoto & Nishimura, 2004). In these models, turbulence is not resolved and a model for high-frequency velocity fluctuations is imperative. However, the importance of such a model is less clear for LES, as the large scale instantaneous turbulent flow is provided as a solution of the flow solver. In fact, Dupont et al. (2013) concluded that the SGS velocities have a negligible effect on particle trajectories. Moreover, Z. Wang et al. (2019) did not consider the SGS velocities when modeling saltation with an LES solver. The impact of SGS velocities on particle trajectories may also depend on the SGS model employed, even though there are no works in the literature regarding this question. In this work, the effect of the SGS turbulence features on the resolved wind velocity field is modeled with one of the most advanced SGS closure schemes, the LASD (Bou-Zeid et al., 2005). Thus, the effect of the SGS velocities on particle motion is assumed to be negligible and not taken into account.

The effect of snow sublimation is also neglected in this study. This simplifies the analysis and avoids the computational cost of solving the thermodynamic interaction between the particles and the air. Recent studies have shown that snow sublimation can be significant in the saltation layer, despite the high values of relative humidity

(Sigmund et al., 2021; Z. Wang et al., 2019). Therefore, the modeling of particle sublimation is particularly important when assessing heat and water vapor transport in the atmosphere during drifting snow events. However, this is outside the scope of this study. The effect of snow sublimation on particle dynamics itself is restricted to a reduction in particles size and to an increase in particles sphericity.

The feedback of particle motion on flow momentum is modeled through a source term,  $S_i$  [ $\text{N m}^{-3}$ ], in the Navier-Stokes equations.  $S_i$  is given by the total drag force induced by the particles, corresponding to the sum of  $-D_i$ , per unit volume. The contribution of each particle is linearly extrapolated to the nearest eight grid nodes where LES is resolved.

Periodic boundary conditions are applied to particles exiting the domain through its vertical walls. Particles that reach the top boundary are assumed to leave the domain and those impacting the bottom boundary (erodible bed) may rebound and eject other grains as described in Section 2.3.

Different studies have been conducted with previous and current versions of this model concerning snow saltation variability (Groot Zwaaftink et al., 2014), drifting snow sublimation (Sharma et al., 2018; Sigmund et al., 2021) and preferential deposition over hills (Comola, Giometto, et al., 2019). A detailed description of the model algorithm and a comparison between simulation results and field/wind tunnel measurements can be found in these works.

### 2.3. Surface Processes

The interaction between surface grains, the wind flow and particles impacting the bed is described by three main processes: aerodynamic entrainment, rebound and splash. These surface processes are modeled with statistical models based on physical principles and experimental correlations, as proposed by Groot Zwaaftink et al. (2014) and further developed by Comola and Lehning (2017).

This approach reduces the computational cost associated with the direct numerical simulation of particle interactions within the granular bed. Saltation models based on the Discrete Element Method (DEM) simulate these complex interactions, but are not suitable for simulating particle transport over large computational domains (Comola, Gaume, et al., 2019; Durán et al., 2012; Pähzt et al., 2015).

#### 2.3.1. Aerodynamic Entrainment

When a fluid flows over a granular and erodible bed, surface particles can be moved and eventually lifted by the flow. This process is called aerodynamic entrainment and occurs when the fluid surface shear stress grows above a given threshold. This threshold, that defines the start of wind erosion, is estimated by considering the forces applied on a grain laying on the bed and by performing a balance of angular momentum. The quantity of interest is the minimum aerodynamic force that makes the grain rotate over its leeward point of contact with the underlying grains and, eventually, leads to an uplift of the grain.

In general, this threshold shear stress is modeled as a mean quantity, related to the instantaneous aerodynamic force by a parameterization. Bagnold (1941) named it the fluid threshold,  $\tau_{ft}$  [Pa]. Considering particle weight, buoyancy and drag, he proposed the following well known expression:

$$\tau_{ft} = A^2 (\rho_p - \rho_f) gd \quad (4)$$

where  $A$  is the fluid threshold coefficient, which depends on different flow and particle characteristics. Chepil (1959) deduced an expression for  $A$ , function of the turbulence intensity, particle geometry and drag coefficient, estimated by a series of experiments developed with sand and soil grains. Bagnold (1941) proposed  $A = 0.1$  for sand beds, after a series of wind tunnel and field experiments. A higher value is expected for very small particles like dust. In this case, the granular surface is not aerodynamically rough and a thin viscous sub-layer is present close to the surface, which limits the transport of flow momentum to the bed. Different criteria have been proposed to define the onset of aerodynamic entrainment. A summary of the latest developments can be found in Pähzt et al. (2020).

Interparticle forces, as the van der Waals and electrostatic forces and those induced by interparticle bonds, also play a role in the aerodynamic entrainment of cohesive materials as snow or moist soils (Schmidt, 1980; Shao & Lu, 2000). However, the quantification of such forces is still a challenge. The contribution of interparticle ice bonds

in the calculation of the fluid threshold is of special interest when studying the erosion of snow covered surfaces and was firstly addressed by Schmidt (1980). However, for common interparticle bond radius, the values estimated for  $\tau_{ft}$  were too large for pure aerodynamic entrainment of snow particles to occur. Other authors, as Lehning et al. (2000) and Clifton et al. (2006), used the same approach suggested by Schmidt (1980), but adjusted the bond properties and empirical constants to improve the agreement with wind tunnel tests performed with natural snow beds. The values for  $\tau_{ft}$  obtained during wind tunnel and field experiments are lower than those deduced by Schmidt (1980), possibly because patches of loose snow grains are always present over dry snow surfaces. These grains can be easily lifted by the flow and contribute to the development of saltation by further ejecting other particles. Moreover, bed microtopography can also induce local peaks in shear stress, leading to the preferential entrainment of grains more exposed to the airflow. The contribution of interparticle cohesion to the fluid threshold can also be taken into account by adjusting the value of the fluid threshold coefficient. For example, Clifton et al. (2006) proposed a value of  $A = 0.18$  from fitting Equation 4 to wind tunnel measurements developed with different snow surfaces.

In light of the challenges and uncertainties to correctly quantify the effect of interparticle forces on the fluid threshold, these forces are not taken into account in the calculation of  $\tau_{ft}$ . Hence,  $\tau_{ft}$  is computed from Equation 4, considering the grain mean diameter,  $\langle d \rangle$  [m], and a constant value for  $A$  equal to 0.1 as proposed by Bagnold (1941). This is a simpler approach suitable to study steady state saltation, where the contribution of aerodynamic entrainment is expected to be negligible in comparison to rebound/splash entrainment (Kok et al., 2012). Indeed, for non-cohesive materials like sand, it is well known that the surface shear stress,  $\tau_s$  [Pa], stays below the fluid threshold during saltation events, which strongly reduces the occurrence of aerodynamic entrainment (e.g., Bagnold, 1941; Owen, 1964).  $\tau_s$  is related to the surface friction velocity,  $u_{*,s}$  [ $\text{m s}^{-1}$ ], by its definition:  $\tau_s = \rho_f u_{*,s}^2$ . The surface friction velocity differs from the imposed friction velocity,  $u_*$ , after saltation onset and the consequent exchange of momentum from the fluid to the particles. For cohesive material like snow, wind tunnel measurements performed by Paterna et al. (2017) have also shown the predominance of rebound/splash mechanisms over aerodynamic entrainment when the wind strength is sufficiently strong for steady state saltation to develop. Naturally, when studying intermittent saltation, a more accurate description of the fluid threshold is required.

The number of grains entrained per unit area per unit time, defined as the aerodynamic entrainment rate,  $N_{ae}$  [ $\text{m}^{-2} \text{s}^{-1}$ ], is computed using the expression proposed by Anderson and Haff (1991):

$$N_{ae} = \eta (\tau_s - \tau_{ft}) \quad (5)$$

where  $\eta$  [ $\text{N}^{-1} \text{s}^{-1}$ ] is the entrainment coefficient, computed with the expression proposed by Doorschot and Lehning (2002):

$$\eta = \frac{C_{ae}}{8\pi \langle d \rangle^2} \quad (6)$$

where the coefficient  $C_{ae}$  [ $\text{m}^2 \text{N}^{-1} \text{s}^{-1}$ ] is set to  $1.5 \text{ m}^2 \text{ N}^{-1} \text{ s}^{-1}$  (Groot Zwaftink et al., 2014). As we are interested in modeling transport limited saltation - a saltation regime for which the amount of saltating particles is only limited by the availability of wind momentum (Kok et al., 2012) - the initial particle concentration at the surface is considered high enough so that there is never a shortage in the supply of erodible particles. However, this is not always the case in snow covered regions, where thin erodible snow layers can exist on top of hard and sintered snow.

In the model, entrained particles start their trajectory at a height of four times the mean grain diameter. The initial velocity and vertical angle of ejection are defined according to a lognormal distribution as described in Clifton and Lehning (2008). The mean and standard deviation of the distribution are computed with the expressions presented in Table 1. The horizontal angle of ejection is given by the horizontal flow direction.

### 2.3.2. Rebound

After impacting the surface, a grain may rebound and eject other particles laying on the bed. The probability of rebound,  $P_r$ , is described by the expression proposed by Anderson and Haff (1991):

$$P_r = P_m [1 - \exp(-\gamma |u_{p,I}|)] \quad (7)$$

**Table 1**

*Initial Velocity of Aerodynamically Entrained, Splashed and Rebounding Grains: Distribution Type, Mean and Standard Deviation*

	Distribution	Mean	Std.	References
<b>Aerodynamic entrainment</b>				
Velocity magnitude	Lognormal	$3.5u_*$	$2.5u_*$	Clifton and Lehning (2008)
Vertical angle <sup>(a)</sup>	Lognormal	$75 - 55 \left[ 1 - \exp \left( -\frac{d}{175 \times 10^{-6}} \right) \right]$	15	Clifton and Lehning (2008)
<b>Rebound</b>				
Velocity magnitude	-	$\sqrt{\epsilon_r}  u_{p,I} $	-	Kok and Renno (2009)
Vertical angle <sup>(a)</sup>	Exponential	45	-	Kok and Renno (2009)
<b>Splash</b>				
Velocity magnitude	Exponential	$0.25  u_{p,I} ^{0.3}$	-	Sharma et al. (2018)
Vertical angle <sup>(a)</sup>	Exponential	50	-	Rice et al. (1995, 1996)
Horizontal angle <sup>(b)</sup>	Normal	0	15	Xing and He (2013)

*Note.* Velocities are in units of  $\text{m s}^{-1}$ , angles are in degrees and the grain size is in meters.

<sup>(a)</sup> Measured from a horizontal plane (downwind between  $0^\circ$  and  $90^\circ$ ).

<sup>(b)</sup> Measured from the plane of particle impact.

where  $P_m$  is the maximum probability of rebound, equal to 0.9 as proposed by Groot Zwaftink et al. (2014) for snow particles,  $\gamma [\text{s m}^{-1}]$  is a constant set to  $2 \text{ s m}^{-1}$  (Anderson & Haff, 1991) and  $|u_{p,I}| [\text{m s}^{-1}]$  is the particle velocity at impact.

The velocity of rebound,  $|u_{p,R}| [\text{m s}^{-1}]$  is given by  $|u_{p,R}| = \sqrt{\epsilon_r} |u_{p,I}|$ , where  $\epsilon_r$  is the fraction of kinetic energy retained by the rebounding grain (restitution coefficient). Saltation models have shown to be highly sensitive to the value of  $\epsilon_r$ , which greatly depends on the particle elastic properties (Kok & Renno, 2009). Experiments developed with sand showed that  $\epsilon_r$  varies according to a normal distribution (D. Wang et al., 2008). Although the restitution coefficient for snow particles is more uncertain, experiments have not suggested a significant deviation from the values obtained for sand grains (Nalpanis et al., 1993).

The horizontal angle of rebound is given by the horizontal flow direction and the vertical angle is computed from an exponential distribution. Further details are presented in Table 1.

### 2.3.3. Splash

When a grain impacts the bed, it can eject several grains initially at rest. This process, named splash or ejection, is the main driver of particle motion during steady state saltation (Kok et al., 2012; Paterna et al., 2017). As flow momentum decreases near the surface due to particle drag, aerodynamic entrainment is highly compromised after the start of saltation. Particles impacting the ground become the main source of momentum as they travel from high momentum regions to the surface.

Numerous statistical splash functions have been proposed to estimate the number of ejected grains,  $N$ , and their initial velocity,  $|u_{p,o}| [\text{m s}^{-1}]$ , as a function of the impacting grain velocity,  $|u_{p,I}|$ , and mass,  $m_I [\text{kg}]$  (e.g., Anderson & Haff, 1988; McEwan & Willetts, 1991). In this work, the number of ejected grains is computed from energy and momentum conservation laws, as proposed by Kok and Renno (2009) and adapted by Comola and Lehning (2017) to take into account the effect of mixed-sized grains and interparticle cohesion.

The impacting grain and the bed are regarded as an isolated system, for which energy and momentum conservation is applied. A fraction of the kinetic energy and momentum,  $\epsilon_r$  and  $\mu_r$ , respectively, is kept by the impacting grain leading to its rebound. The remaining fraction is only partly transferred to the ejected grains, as a fraction of the impacting energy and momentum,  $\epsilon_f$  and  $\mu_f$ , respectively, leads to the rearrangement of surface grains and, consequently, to friction related losses.

Both the energy and momentum conservation equations are solved for  $N$  by statistically representing the kinetic energy and momentum of the ejected grains by their mean values. Only the horizontal direction of the

**Table 2**  
*Parameters of the Splash Model*

Parameter	Values used in the model	References
$\epsilon_r$	0.25	Rice et al. (1995); D.Wang et al. (2008)
$\epsilon_f$	$0.96(1 - P_r \epsilon_r)$	Ammi et al. (2009)
$\mu_r$	$\sqrt{\epsilon_r}$	-
$\mu_f$	0.4	Rice et al. (1995)
$r_E$	0	-
$r_M$	0	-
$\langle \cos\alpha \rangle$	0.75	Rice et al. (1995)
$\langle \cos\beta \rangle$	0.96	Xing and He (2013)
$\phi$ [J] <sup>(a)</sup>	$10^{-10}, 5 \times 10^{-10}, 5 \times 10^{-9}$	Gauer (2001)

<sup>(a)</sup> Values obtained for ice particles.  $\phi = 0$  J is considered for loose grains.

momentum equation is taken into account as the vertical component of the impact velocity is relatively small (Bagnold, 1941). Comola and Lehning (2017) arrived to the following expressions:

$$N_E = \frac{(1 - P_r \epsilon_r - \epsilon_f) m_I u_{p,I}^2}{\langle m \rangle \langle u_{p,o}^2 \rangle + r_E \sigma_m \sigma_{u_{p,o}^2} + 2\phi} \quad (8a)$$

$$N_M = \frac{(1 - P_r \mu_r - \mu_f) m_I u_{p,I} \cos\alpha_I}{\langle m \rangle \langle u_{p,o} \rangle \langle \cos\alpha \rangle \langle \cos\beta \rangle + r_M \sigma_m \sigma_{u_{p,o}}} \quad (8b)$$

where  $N_E$  and  $N_M$  denote the number of ejected grains computed by the energy and momentum equations, respectively. The quantities within angle brackets represent average values,  $m$  [kg] being the mass of an ejected grain,  $\alpha$  [ $^\circ$ ] the vertical angle of ejection and  $\beta$  [ $^\circ$ ] the horizontal angle of ejection measured from the plane of impact (in the above equations, both  $\alpha$  and  $\beta$  are assumed statistically independent).  $\sigma_m$  [kg],  $\sigma_{u_{p,o}}$  [ $\text{m s}^{-1}$ ] and  $\sigma_{u_{p,o}^2}$  [ $\text{m}^2 \text{s}^{-2}$ ] denote the standard deviation of  $m$ ,  $u_{p,o}$  and  $u_{p,o}^2$ , respectively.  $\alpha_I$  [ $^\circ$ ] is the vertical angle of impact,  $r_E$  and  $r_M$  are the correlation coefficients between  $m$  and  $u_{p,o}^2$  and between  $m$  and  $u_{p,o}$ , respectively, and  $\phi$  [J] is the energy required to break the cohesive bonds between each ejected grain and the surrounding ones. The modulus symbol in both  $u_{p,o}$  and  $u_{p,I}$  was suppressed for simplicity.

The number of ejected grains is then given by the minimum value between  $N_E$  and  $N_M$ , which guarantees that neither energy nor momentum is created. The number of ejected grains is expected to be restricted by momentum conservation when the bed is constituted by loose grains (Kok & Renno, 2009). However, this is not always obtained when interparticle forces are present (Comola & Lehning, 2017; Shao et al., 1993).

The main difference between the splash dynamics of sand and snow particles lies indeed in the nature of the interparticle forces (Comola & Lehning, 2017). In snow, they arise from ice bonds among neighboring particle, while in sand they are caused by the occasional presence of water menisci. Several parameters in the splash functions are expected to depend on the material properties, such as the ejection velocity of splashed grains and the restitution coefficient,  $\epsilon_r$ . In the particular case of snow, metamorphic changes in the snow surface may also induce variations in the parameters. Moreover, in the work of Doorschot et al. (2004), the authors question the occurrence of rebound and splash for fresh snow. Despite these differences, the studies of Nalpanis et al. (1993) and Nishimura and Hunt (2000) have shown some similarities between the main snow and sand splash parameters. The parameters' values considered in this study are therefore mainly based on sand experiments (e.g., Anderson & Haff, 1988, 1991; Kok & Renno, 2009; Rice et al., 1995, 1996; Xing & He, 2013). The velocity and angle of ejection are defined according to specific probability distributions (Table 1) and the parameters  $\epsilon_r$ ,  $\epsilon_f$ ,  $\mu_r$ ,  $\mu_f$ ,  $r_E$ ,  $r_M$ ,  $\langle \cos\alpha \rangle$  and  $\langle \cos\beta \rangle$  are assumed constant (Table 2). Sensitivity analysis carried out by Comola and Lehning (2017) revealed that the splash model used in this study is robust to variations of up to  $\pm 20\%$  in the model parameters. Additional studies on the splash mechanics of natural snow (see e.g., Araoka & Maeno, 1981; Nishimura & Hunt, 2000) would ultimately help reducing the model uncertainties.

The correlation coefficients,  $r_E$  and  $r_M$ , are set to zero, as in Comola and Lehning (2017). The mean and standard deviation of the mass of ejected grains are computed assuming equally sized grains or a lognormal distribution for the grain diameter (Colbeck, 1986). Finally, the cohesion energy,  $\phi$ , is set to different figures throughout the simulations according to the range proposed by Gauer (2001) and investigated by Comola and Lehning (2017).

### 3. Numerical Setup

#### 3.1. General Settings

The computational domain is a cube of 6.4 m side length. It models the near surface atmospheric flow over a flat erodible bed. The domain is relatively short in both horizontal directions, especially in the streamwise one. This is partially compensated by applying periodic boundary conditions. However, the use of a longer domain is necessary for the consistent development of large coherent structures observed in experimental and numerical boundary layer studies (Munters et al., 2016). Even though longer domains are imperative for a proper comparison with experimental data, a cubic domain was considered adequate for the study of steady state saltation developed in this paper. Moreover, it greatly reduces the computational time.

The domain is discretized in 64 cells of equal size in the streamwise and crosswise directions. The vertical direction is discretized in 128 cells using a hyperbolic function. The hyperbolic function guarantees a more refined mesh close to the bottom boundary, with an approximately constant thickness of 1 cm in the first 15 cm. The first grid center point is placed in the logarithmic sublayer, at  $\sim 0.5$  cm height.

The simulations are performed over a total of 350 s to allow the development of steady state saltation. The time step is set to  $5 \times 10^{-5}$  s for both the flow and particle solvers. The flow is allowed to develop over 25 s prior to the start of surface erosion.

The initial streamwise component of the velocity field is given by a logarithmic profile, function of  $u_*$  and of the roughness length,  $z_0$  [m]. The roughness length is assumed constant along the surface and equal to  $10^{-5}$  m. The initial crosswise and vertical velocity components are set to zero. White noise is added to all initial velocity components to accelerate the development of a fully developed turbulent flow.

The fluid density and kinematic viscosity are set to  $\rho_f = 1.34 \text{ kg m}^{-3}$  and  $\nu_f = 1.24 \times 10^{-5} \text{ m}^2 \text{ s}^{-1}$ , respectively. Particles are modeled as ice spheres with density  $\rho_p = 918.4 \text{ kg m}^{-3}$ . The top of the erodible surface is defined at a height  $z = 0$  m and particle size is assumed uniform or defined by a lognormal distribution, characterized by the grain mean diameter,  $\langle d \rangle$ , and standard deviation,  $\sigma_d$  [m].

In order to reduce the computational cost of the simulations, particles are not modeled individually but grouped in parcels, constituted by particles of equal size that follow the same trajectory. Particles from the same parcel were aerodynamically entrained at the same surface location and time step, or were ejected from the same impact event. The number of particles per parcel can assume a value between 5,000 and 250,000. As a consequence, the number of parcels aloft varies from 5,000 to 20,000 during steady state conditions, for friction velocities ranging from 0.4 to 0.8 m s<sup>-1</sup>. This assumption is considered reasonable for the analysis of time-averaged quantities performed in this work.

#### 3.2. Simulation Details

In order to study the effect of friction velocity, mean grain size, size distribution and cohesion energy on saltation dynamics, four groups of simulations are performed - S1 to S4 - for which different values of  $u_*$ ,  $\langle d \rangle$ ,  $\sigma_d$  and  $\phi$  are considered. The parameters used in each simulation group are summarized in Table 3.

In simulations S1 and S2, a bed of equally sized ( $\sigma_d = 0 \mu\text{m}$ ) and loose grains ( $\phi = 0 \text{ J}$ ) is modeled. In S1, the effect of the imposed friction velocity is studied while keeping the remaining parameters unchanged. In S2, different values for the grain diameter,  $\langle d \rangle$ , are tested. In simulations S3 and S4, a bed of mixed-sized grains is modeled by describing the grain size by a lognormal distribution. In S3, the effect of the standard deviation of the distribution,  $\sigma_d$ , on steady state saltation is analyzed. Finally, in S4, interparticle forces are assumed between surface grains and different values for the cohesion energy,  $\phi$ , are tested. Different values for  $u_*$  are also considered in simulations S2 to S4. The fluid threshold coefficient is set to  $A = 0.1$  and the splash model parameters are set to the values presented in Table 2.

**Table 3**  
*Simulation Input Parameters*

	Description	$u_*$ [ $\text{m s}^{-1}$ ]	$\langle d \rangle [\mu\text{m}]$	$\sigma_d [\mu\text{m}]$	$\phi [\text{J}]$
S1	Effect of friction velocity	0.3–0.8	200	0	0
S2	Effect of mean grain diameter	0.4–0.8	100, 300, 400	0	0
S3	Effect of size distribution	0.4–0.8	200	100, 200	0
S4	Effect of cohesion	0.4–0.8	200	100	$10^{-10}, 5 \times 10^{-10}, 5 \times 10^{-9}$

### 3.3. Data Post-Processing

The vertical profiles of particle concentration, mean particle streamwise velocity and particle mass flux are computed by dividing the computational domain in horizontal layers of thickness  $\Delta z_k$  [m].

The particle concentration,  $c$  [ $\text{kg m}^{-3}$ ], is given by

$$c(z_k) = \frac{\sum_{n=1}^{N_k} m_n}{L_x L_y \Delta z_k} \quad (9)$$

where  $N_k$  is the number of particles in the horizontal layer with mean height  $z_k$  [m],  $m_n$  [kg] is the mass of the  $n^{\text{th}}$  particle,  $L_x$  [m] is the domain length and  $L_y$  [m] is the domain width.

The mean particle velocity in the streamwise direction,  $\langle u_{p,1} \rangle$  [ $\text{m s}^{-1}$ ], is given by the arithmetic mean. The particle mass flux,  $q$  [ $\text{kg m}^{-2} \text{s}^{-1}$ ], is given by the product of the particle concentration and the mass-weighted average particle streamwise velocity, yielding

$$q(z_k) = \frac{\sum_{n=1}^{N_k} m_n u_{p,1,n}}{L_x L_y \Delta z_k} \quad (10)$$

where  $u_{p,1,n}$  [ $\text{m s}^{-1}$ ] is the streamwise velocity of the  $n^{\text{th}}$  particle in layer  $k$ .

The integrated mass flux of saltating particles,  $Q$  [ $\text{kg m}^{-1} \text{s}^{-1}$ ] is computed by integrating particle mass flux,  $q$ , along the height, from the surface to 15 cm. The last 100 s of each simulation are used to compute the time-averaged values of  $c$ ,  $\langle u_{p,1} \rangle$ ,  $q$  and  $Q$ . During this time interval (250–350 s), the changes in total mass of particles aloft are negligible and saltation is assumed to be in steady state.

The surface friction velocity,  $u_{*,s}$ , at each time step is obtained by averaging over the surface. The time-averaged value obtained for the last 100 s of each simulation is defined as the equilibrium surface friction velocity,  $u_{*,eq}$  [ $\text{m s}^{-1}$ ].

## 4. Results and Discussion

In this section, the results are presented and discussed. Results obtained with simulations S1 to S4 are analyzed in Sections 4.1 to 4.4, respectively. Moreover, a comparison with existing saltation models and with the conclusions drawn from the latest wind tunnel and field experiments is presented.

### 4.1. The Effect of Friction Velocity

In simulations S1, a bed of equally sized and loose grains with a diameter of 200  $\mu\text{m}$  is modeled. The streamwise wind speed profiles are presented in Figure 1. They are computed by averaging the streamwise velocity along horizontal planes. The profiles are time-averaged over the first 25 s and over the last 100 s of each simulation (before saltation onset and during steady state saltation). As expected, the resulting wind speed is lower for the latter, as the saltation layer acts on the flow as an additional sink of momentum.

The velocity profiles obtained during steady state saltation intercept in a point at  $\sim 7$  mm above the surface (inset in Figure 1). This characteristic feature of steady state saltation was originally observed by Bagnold (1941) when performing wind tunnel experiments. This point is defined as the focus point. Previous saltation models have

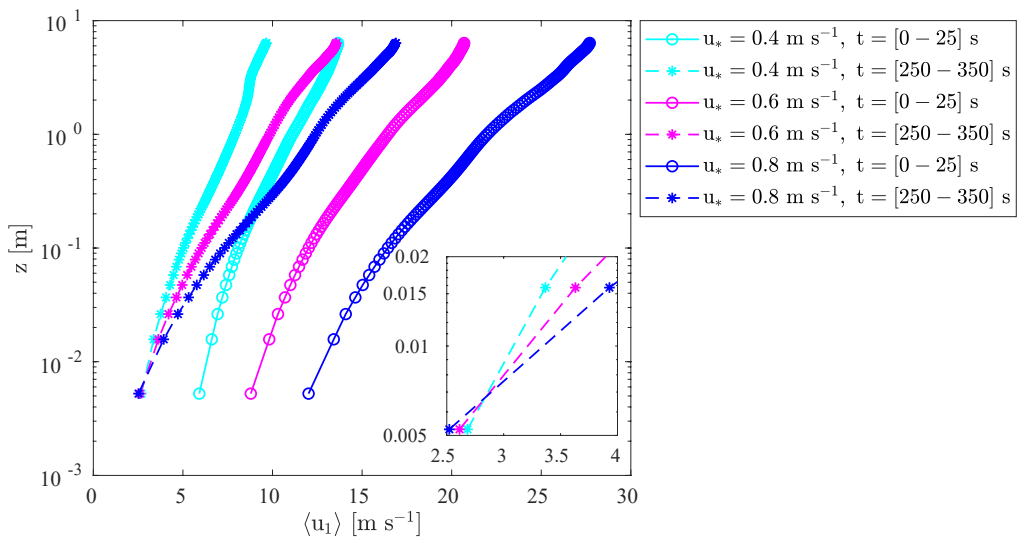


**Figure 1.** Vertical profiles of mean streamwise wind speed obtained before saltation onset and during steady state saltation (simulations S1). The inset is a zoom-in to the near surface region during saltation.

characterized the wind velocity profile in the saltation layer using a logarithmic profile and have assumed the existence of a focus point (e.g., Pomeroy & Gray, 1990). This greatly simplifies the description of the velocity field in the saltation layer and, consequently, the theoretical modeling of saltation. Numerical models based on parameterizations of splash entrainment have also reproduced this characteristic feature (Kok et al., 2012). The height of the focus point is expected to vary between 1 and 10 mm (Bagnold, 1941; Kok et al., 2012). In order to accurately assess its location, a more refined mesh near the surface would have to be employed.

An equivalent surface roughness, characteristic of each saltation layer, can be estimated from the velocity profiles obtained during steady state saltation (Dupont et al., 2013). By extending the velocity profiles down to the wall, zero velocity is attained at greater heights as  $u_*$  increases. Hence, the equivalent surface roughness increases with  $u_*$ . This is related to an enhanced momentum exchange between the fluid flow and the particles aloft when  $u_*$  increases. Therefore, it is ultimately related to the increase in particle mass flux.

The time-averaged vertical profiles of particle mass flux, concentration and mean streamwise velocity are presented in Figures 2a–2c. The average is performed over the last 100 s of each simulation. Particle mass flux decreases with height and increases with  $u_*$  (Figure 2a), as previously observed in field measurements (Nishimura et al., 2014). A similar trend is observed for particle concentration (Figure 2b). Several saltation models have assumed an exponential decay for the vertical profile of particle mass flux of the form  $q(z) = q_m \exp(-z/l_r)$ , where  $l_r$  [m] is a reference height, commonly related to the height of the saltation layer, and  $q_m$  [ $\text{kg m}^{-2} \text{s}^{-1}$ ] is given by the ratio of the integrated mass flux,  $Q$ , to the reference height,  $l_r$  (Clifton et al., 2006; Martin & Kok, 2017; Nishimura & Hunt, 2000; Vionnet et al., 2014). Some saltation models (Clifton et al., 2006; Vionnet et al., 2014) define  $l_r = u_*^2/(\lambda g)$ , where  $\lambda = 0.45$ , as proposed by Nishimura and Hunt (2000) after wind tunnel experiments developed with fine-grained natural snow. We present the vertical profiles of particle mass flux in a semi-logarithmic scale in Figure 3. The fitting of the simulation results to an exponential decay is also presented. The fit is performed up to a height of 3, 5 and 14 cm for  $u_*$  equal to 0.4, 0.6 and 0.8  $\text{m s}^{-1}$ , respectively. Moreover, the near surface value of  $q$  is neglected in the fit. The reference height,  $l_r$ , obtained from the fit and from the expression proposed by Nishimura and Hunt (2000) is also indicated at each exponential curve. It can be seen that particle mass flux decreases exponentially with height in the first centimeters above the ground. Moreover, a slight increase of  $l_r$  with  $u_*$  is obtained, which implies a weak variation of the saltation layer height with  $u_*$ . This trend was also obtained by Nalpanis et al. (1993) and Martin and Kok (2017) after wind tunnel and field experiments, respectively, developed with sand. However, it contrasts with the stronger increase proposed by Nishimura and Hunt (2000).

Simpler saltation models assume a constant particle mass flux in the saltation layer,  $\langle q \rangle$  [ $\text{kg m}^{-2} \text{s}^{-1}$ ], so that  $Q = \langle q \rangle h_s$ , where  $h_s$  [m] is the height of the saltation layer (Pomeroy & Gray, 1990). Particle mass flux is

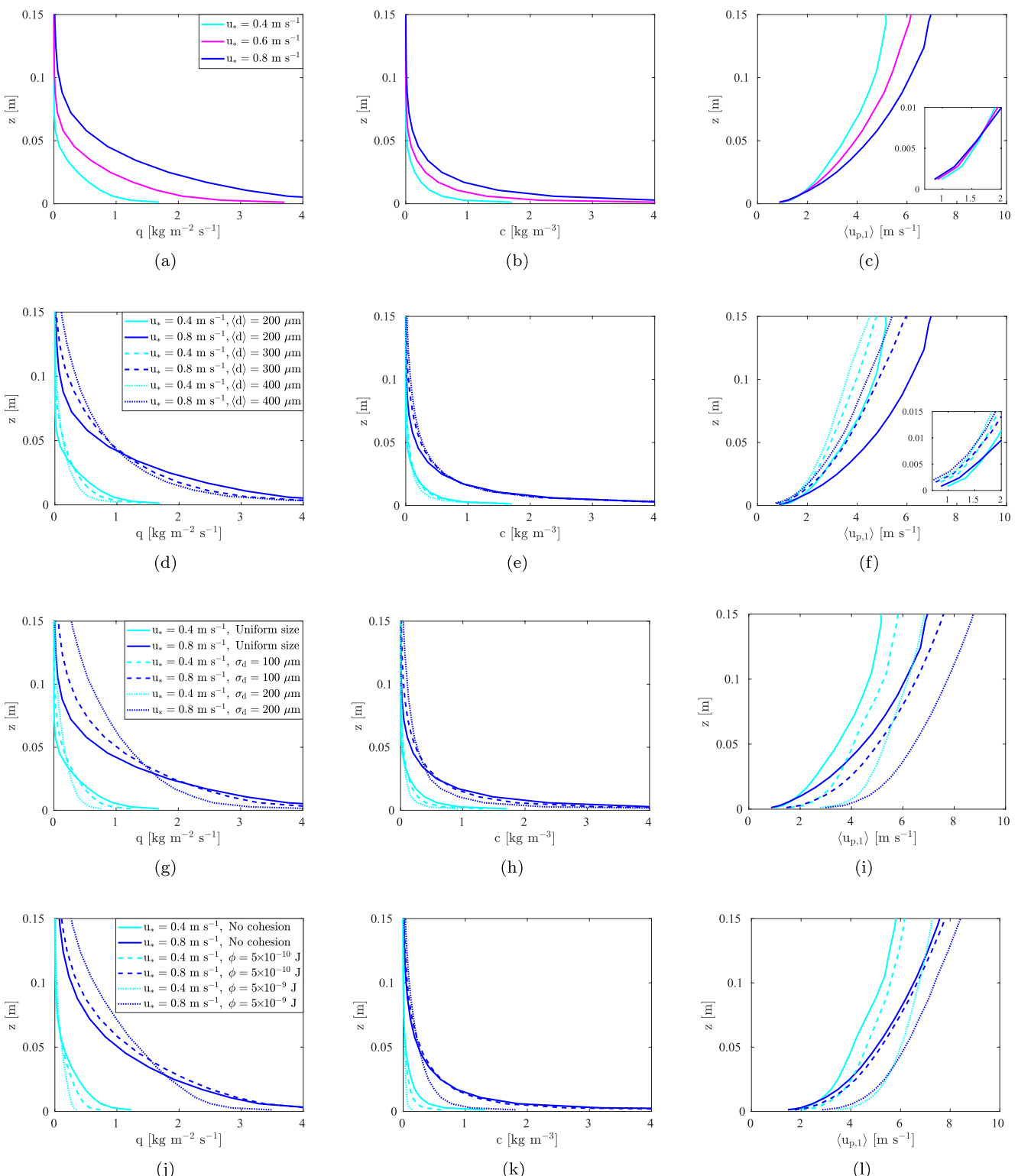


**Figure 2.** Vertical profiles of particle mass flux, concentration and streamwise velocity obtained with simulations S1 (a–c), S2 (d–f), S3 (g–i) and S4 (j–l). In (d–i) and (j–l) results from simulations S1 and S3 are presented for comparison, respectively. All values are obtained from surface averages and time averages over the last 100 s of each simulation. The insets in (c and f) are a zoom-in to the near surface region.

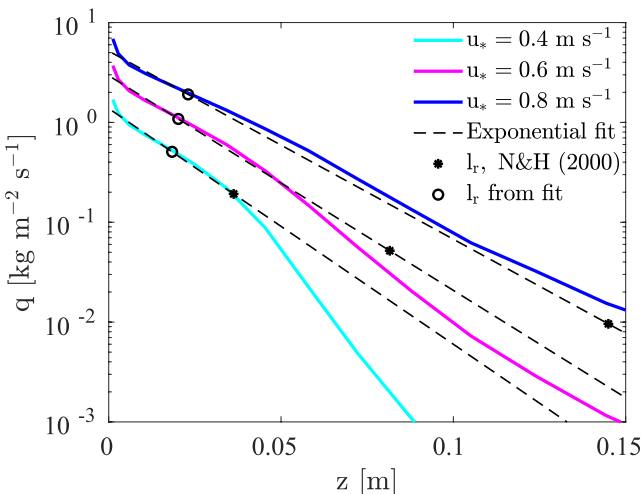


**Figure 3.** Vertical profile of particle mass flux obtained with simulations S1 and fit to exponential decay. The reference height,  $l_r$ , computed from the exponential fit and from the expression proposed by Nishimura and Hunt (2000) (N&H) is indicated at each exponential curve.

given by the product of particle concentration and particle streamwise velocity, as described in Section 3.3. Particle concentration at the saltation layer height is the quantity of interest when modeling snow suspension (e.g., Amory et al., 2015, 2021; Lenaerts et al., 2012; Vionnet et al., 2014). In order to compute it, particle mass flux at  $h_s$  must be known. Taking into account the strong variation of  $q$  with height (Figure 3), the assumption of a mean value will hardly deliver a reasonable estimate of  $q(h_s)$ , even if an accurate description for  $Q$  and  $h_s$  is considered. Different criteria have been proposed to define the height of the saltation layer. They are either based on the mean height of particle trajectories (Owen, 1964), the amount of momentum transported from the fluid to the particles (Dupont et al., 2013), or the exponential fit of the mass flux profile (Martin & Kok, 2017). Due to the lack of consensus in this matter, a precise definition of the saltation layer height is avoided in this work.

Particle streamwise velocity increases with height and  $u_*$  (and, therefore, with wind speed), as shown in Figure 2c. For heights smaller than 1 cm (approximately), the variation of particle streamwise velocity with  $u_*$  is negligible (inset in Figure 2c). This is predicted by existing saltation models (Kok & Renno, 2009) and wind tunnel measurements (Ho et al., 2011). This result is also obtained theoretically, based on the notion that steady state saltation is characterized by a mean replacement capacity equal to one (Kok et al., 2012).

This means that, on average, one grain enters the saltation layer each time an impacting grain fails to rebound. Assuming that saltation is mainly dominated by splash, this condition is met for a given impact velocity, which completely defines the number of ejected grains and the probability of rebound for a given bed type (see Equations 7 and 8). Hence, it follows that the particle speed near the surface is independent of  $u_*$  and rather varies with the bed characteristics. The near surface particle speed is closely linked to the focus point (or Bagnold's focus) observed in the average streamwise wind speed profiles (Figure 1). Saltating particles are accelerated by the flow along their trajectories, therefore, the near surface particle speed can only be approximately invariant with regards to  $u_*$  if the near surface wind speed is also approximately invariant with regards to the same quantity. High above the surface, the wind speed increases as  $u_*$  rises. Hence, a near surface wind speed approximately invariant with  $u_*$  is only obtained if a focus point is visible close to the surface, below which the wind speed decreases as  $u_*$  increases.

Some of the snow saltation models implemented in atmospheric models (Pomeroy & Gray, 1990; Vionnet et al., 2014) assume that the mean particle streamwise velocity in the saltation layer is invariant with  $u_*$ . In addition, they assume that the saltation layer height varies from 1 to 5 cm (or from 2 to 6 cm) for  $u_*$  varying from 0.4 to 0.8  $\text{m s}^{-1}$ , respectively. Indeed, our results show that the mean particle speed does not vary with  $u_*$  in the first centimeter above the ground (inset in Figure 2c). However, this is not considered representative of the whole saltation layer. The wind tunnel measurements of Ho et al. (2011) revealed a negligible increase of particle speed with  $u_*$  up to a height of 4 cm. However, the field measurements of Nishimura et al. (2014) showed a clear increase of particle speed with friction velocity between 1 and 10 cm height. In large scale models, the correct estimate of particle speed is required for the calculation of particle concentration, which is used as a lower boundary condition for suspension.

The surface friction velocity,  $u_{*,s}$ , as a function of time is presented in Figure 4. The fluid threshold friction velocity,  $u_{*,ft}$  [ $\text{m s}^{-1}$ ], related to the fluid threshold shear stress by  $\tau_{ft} = \rho_f u_{*,ft}^2$ , is also plotted as a reference.  $u_{*,s}$  strongly decreases immediately after the start of surface erosion ( $t = 25$  s). It tends to an equilibrium value - the equilibrium surface friction velocity,  $u_{*,eq}$ . A small reduction of  $u_{*,eq}$  is obtained when the imposed friction velocity,  $u_*$ , increases (inset in Figure 4). The numerical model COMSALT proposed by Kok and Renno (2009) also predicts this trend for a bed with uniform grain size (Kok et al., 2012). However, they predicted a stronger reduction than that presented in the inset in Figure 4. The wind tunnel experiments performed by Walter et al. (2014) revealed a non-monotonic evolution of  $u_{*,eq}$  with  $u_*$ . During the experiments,  $u_*$  was continuously increased above the fluid threshold friction velocity. As a result, the measured  $u_{*,eq}$  firstly reduced and then increased. In general, a relatively small variation of  $u_{*,eq}$  with  $u_*$  and a relatively large standard deviation of the measurements were obtained,

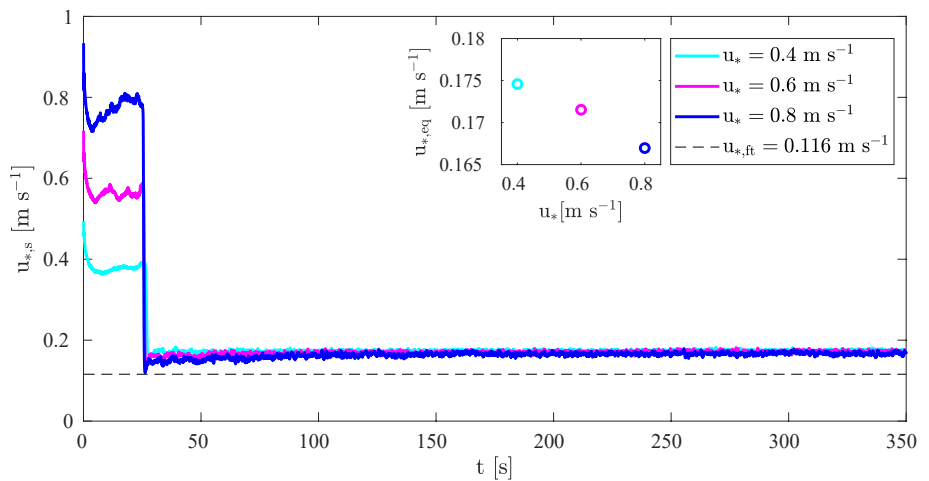


**Figure 4.** Surface friction velocity obtained with simulations S1. The fluid threshold friction velocity is also presented as a reference. In these simulations, saltation is allowed to develop after the first 25 s. The equilibrium friction velocity is presented in the inset.

which may be partially related to changes in the snow cover during the experiments. Based on these results, Walter et al. (2014) considered the assumption of a constant surface friction velocity (function of the grain type but invariant with the wind speed, as proposed by Owen (1964)) a reasonable first-order approximation.

The impact threshold friction velocity,  $u_{*,it}$  [ $m s^{-1}$ ], is generally defined as the minimum friction velocity,  $u_*$ , at which saltation can be sustained after its onset (Bagnold, 1941). In the work of Kok and Renno (2009), the impact threshold friction velocity is assumed equal to the minimum value of  $u_*$  that satisfies the steady state equation. In their model, the equilibrium friction velocity,  $u_{*,eq}$ , tends to the computed  $u_{*,it}$  as  $u_*$  decreases (Kok et al., 2012). Taking into account these results, a simplified approach is followed in this work and  $u_{*,it}$  is given by the value of  $u_{*,eq}$  obtained when  $u_*$  is set to  $0.4 m s^{-1}$  (the minimum friction velocity common to all simulation groups). This approach is considered appropriate taking into account the small variation of  $u_{*,eq}$  with  $u_*$  obtained for most simulations. A more accurate estimation of the impact threshold friction velocity needs further investigation, in particular, a set of simulations at low friction velocities (near the impact and fluid threshold friction velocities) and the analysis of the transition from intermittent to steady state saltation.

The mass of particles aloft per unit surface area varies with time, as presented in Figure 5. The vertical mass flux of particles leaving the surface either through aerodynamic entrainment or splash and the vertical mass flux of

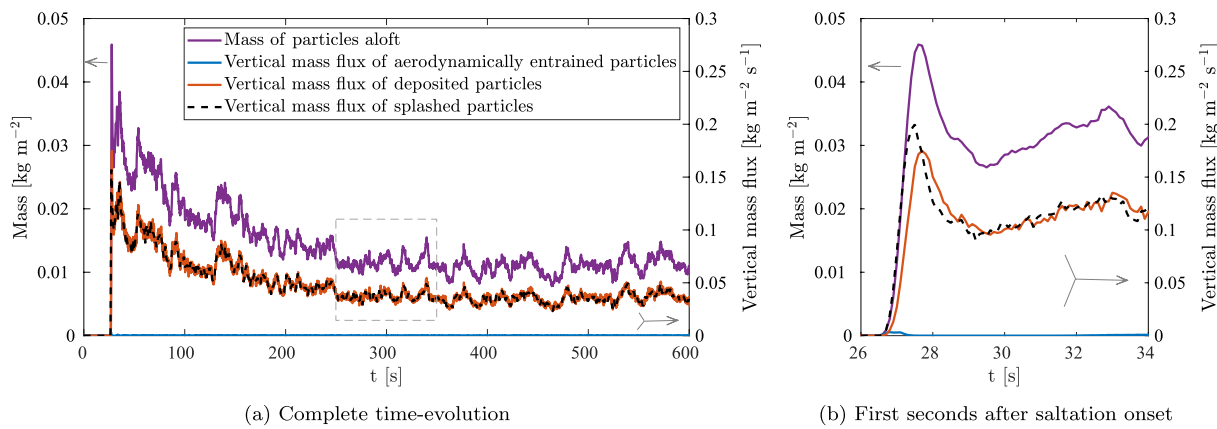


**Figure 5.** Time-evolution of the mass of particles aloft per unit area (purple line). The time-evolution of the vertical mass flux of particles leaving the surface either through aerodynamic entrainment or splash and the vertical mass flux of particles deposited are presented in blue, dashed black and orange, respectively. Results obtained from simulation S1 with  $u_* = 0.4 m s^{-1}$ . The arrows indicate the y-axis corresponding to each curve. The rectangle encloses the time interval used to compute the time-averaged quantities.

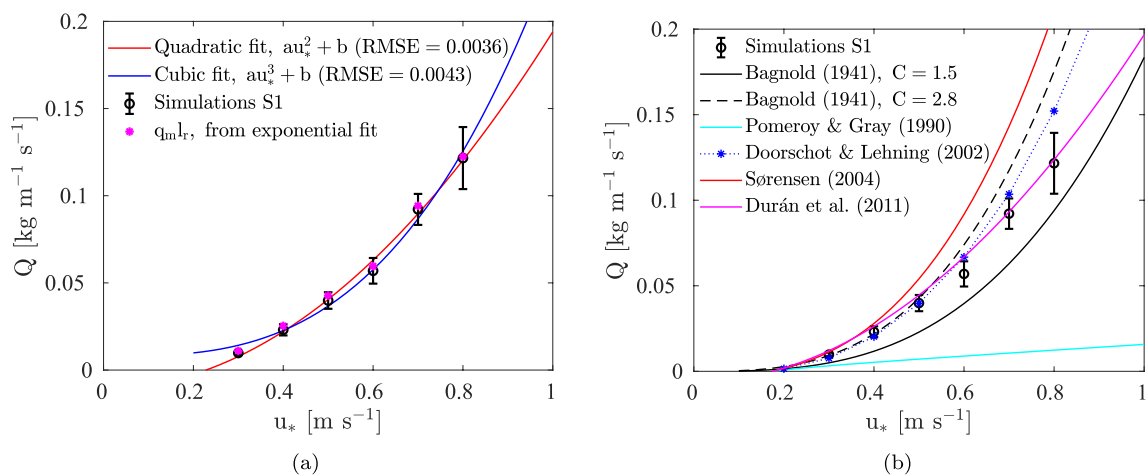


**Figure 6.** Integrated mass flux obtained with simulations S1. The error bar is twice the standard deviation of the results. (a) Fit of simulation results to quadratic and cubic functions (RMSE is the root mean square error of the fit); comparison with the product  $q_{mlr}$ , obtained from the exponential fit of the particle mass flux profile. (b) Comparison with saltation models.

particles deposited due to failure of rebound are also presented. The results were obtained for  $u_* = 0.4 \text{ m s}^{-1}$ . A longer simulation time of 600 s was considered in this case to better illustrate the steady state regime. The evolution shown in the first 350 s is representative of all the simulations performed. At  $t = 25 \text{ s}$ , saltation starts due to aerodynamic entrainment. A sudden increase in the mass of particles aloft is observed, which is consistent with the strong decrease in surface friction velocity presented in Figure 4. The overshoot in particle mass is justified by the surge in the vertical mass flux of particles entering saltation via splash, that overcomes the vertical mass flux of particles leaving the saltation layer through deposition (Figure 5b). The imbalance between the vertical mass flux of splash and deposition drives the variation of mass of particles aloft. When saltation reaches steady state, a dynamic equilibrium between the vertical mass flux of splash and deposition is obtained. Aerodynamic entrainment is much smaller than splash: the vertical mass flux reaches a maximum at saltation onset and then decreases to a steady state value, which is one order of magnitude lower than the vertical mass flux of splash and deposition. In the simulations performed, aerodynamic entrainment occurs during steady state saltation because the surface friction velocity is greater than the specified fluid threshold friction velocity (Figure 4). However, taking into account the relatively small contribution of aerodynamic entrainment to the mass of particles aloft, the correct assessment of the fluid threshold is expected to have a negligible effect on steady state saltation for friction velocities significantly greater than the fluid threshold friction velocity. These results are in agreement with the notion that steady state saltation is dominated by splash and that an equilibrium between splash and failure of rebound should be attained (Kok et al., 2012; Paterna et al., 2017).

The time-averaged integrated mass flux and the corresponding standard deviation are presented in Figure 6. In Figure 6a, the fit between the mean values and a quadratic function is presented, as well as between the mean values and a cubic function. Moreover, the integrated mass flux estimated from fitting the vertical profile of particle mass flux to an exponential function is also shown. In Figure 6b, the results are compared to saltation models proposed by several authors (Bagnold, 1941; Doorschot & Lehning, 2002; Durán et al., 2011; Pomeroy & Gray, 1990; Sørensen, 2004). The results from Doorschot and Lehning (2002) were obtained from the numerical algorithm proposed by the authors. The remaining curves are computed from the equations presented in Table 4.

Equations used to compute the integrated mass flux (as those presented in Table 4) are obtained from the balance of horizontal momentum applied to the saltating particles. The total horizontal force per unit area applied on these particles is equal to the excess shear stress,  $\tau - \tau_s = \rho_f (u_*^2 - u_{*,s}^2)$ , where  $\tau$  [Pa] is the surface shear stress before saltation onset ( $\tau = \rho_f u_*^2$ ). In addition, if particle trajectories are characterized by a representative hop, with length  $L$  [m], in which particles undergo a mean variation of horizontal velocity,  $\Delta u_{ph}$  [ $\text{m s}^{-1}$ ], between lift off and impact with the bed, the integrated mass flux is computed from  $Q = \rho_f (u_*^2 - u_{*,s}^2) L / \Delta u_{ph}$  (e.g., Kok et al., 2012). Different models arise from different assumptions regarding the evolution of  $u_{*,s}$  and  $L / \Delta u_{ph}$ . Following Owen's hypothesis (Owen, 1964), the surface friction velocity,  $u_{*,s}$ , is generally assumed invariant with respect to  $u_*$  and equal to the impact threshold friction velocity,  $u_{*,it}$ . Even though there is no full consensus on

**Table 4**  
*Saltation Models for the Integrated Mass Flux,  $Q$*

Integrated mass flux [ $\text{kg m}^{-1} \text{s}^{-1}$ ]	Constant parameters	References
$Q_{Bag} = C \sqrt{\frac{\langle d \rangle}{d_R} \frac{\rho_f}{g}} u_*^3$	$C = 1.5$ (uniform grains) $C = 2.8$ (highly non-uniform grains)	Bagnold (1941)
$Q_{P&G} = C \frac{\rho_f}{g} u_{*,it} u_* \left( 1 - \frac{u_{*,it}^2}{u_*^2} \right)$	$C = 0.68$	Pomeroy and Gray (1990)
$Q_{S\emptyset} = \frac{\rho_f}{g} u_*^3 \left( 1 - \frac{u_{*,it}^2}{u_*^2} \right) \left( \alpha + \beta \frac{u_{*,it}^2}{u_*^2} + \gamma \frac{u_{*,it}}{u_*} \right)$	$\alpha = 2.6, \beta = 2.5, \gamma = 2.0$ <sup>(a)</sup>	Sørensen (2004)
$Q_{Dur} = C \frac{\rho_f}{g} u_{*,it} u_*^2 \left( 1 - \frac{u_{*,it}^2}{u_*^2} \right)$	$C = 8.5$ <sup>(b)</sup>	Durán et al. (2011)

Note.  $d_R$  is a reference diameter,  $d_R = 250 \times 10^{-6} \text{ m}$ .

<sup>(a)</sup> Constant parameters proposed by Vionnet et al. (2014) from fitting the equation to the experimental measurements of Nishimura and Hunt (2000).

<sup>(b)</sup>  $C$  estimated from Figure 27 in Durán et al. (2011), assuming a packing fraction of the bed,  $\phi_b$ , equal to 0.95.

the validity of this hypothesis and its implications on saltation dynamics (see, for instance, Kok et al. (2012) and Walter et al. (2014)), the fact that the general equation yields  $Q = 0$  when  $u_*$  equals  $u_{*,s}$  favors the use of this simplifying assumption. The quadratic growth of  $Q$  with  $u_*$  is predicted theoretically when both the particle velocity near the surface (and, consequently,  $\Delta u_{ph}$ ) and the representative hop length are considered invariant with  $u_*$  (Durán et al., 2011; Ungar & Haff, 1987). This yields an expression for  $Q$  of the form  $au_*^2 + b$ , which is corroborated by recent field experiments (e.g., Martin & Kok, 2017). The increase of  $Q$  with  $u_*^3$  was early proposed by Bagnold (1941) based on the assumptions that  $L$  is proportional to  $u_*^2$  and that the near surface particle velocity increases linearly with  $u_*$ . This yields an expression for  $Q$  of the form  $au_*^3 + b$ . A cubic expression for the integrated mass flux can also be obtained by assuming that particle velocity near the surface is invariant with  $u_*$ , but considering a linear increase of  $L$  with  $u_*$  (Sørensen, 1991, 2004). However, experiments show that a cubic increase of  $Q$  with  $u_*$  is only likely to happen when saltation develops over rigid beds (Ho et al., 2011).

In Figure 6a, a good agreement is obtained for both polynomial functions, although the quadratic fit is slightly better (root mean square error, RMSE, equal to 0.0036 instead of 0.0043). In fact, for the range of studied friction velocities, small differences between the two functions are obtained. In addition, a good agreement is seen between the integrated mass flux and the product  $q_m l_r$  estimated from fitting the particle mass flux profile to an exponential function (Figure 3). This agreement underlines the importance of an accurate representation of the near surface mass flux profile. Moreover, it reveals that the contribution of the upper region of the saltation layer to the integrated mass flux is negligible.

In Figure 6b, the comparison between simulation results and saltation models is made by assuming an impact threshold friction velocity of  $0.175 \text{ m s}^{-1}$  (the value of  $u_{*,eq}$  obtained for  $u_* = 0.4 \text{ m s}^{-1}$ , as previously discussed). In the models proposed by Pomeroy and Gray (1990), Sørensen (2004) and Durán et al. (2011), the impact threshold friction velocity is a parameter in the integrated mass flux equations which characterizes the erodible bed (Table 4). For friction velocities lower than  $0.6 \text{ m s}^{-1}$ , a good agreement is seen between simulation results and the saltation model proposed by Doorschot and Lehning (2002). At higher friction velocities, the model proposed by Doorschot and Lehning (2002) predicts greater values for  $Q$  and a better agreement is obtained with the expression proposed by Durán et al. (2011).  $Q_{Dur}$  scales with  $u_*^2$ , which is supported by the current simulation results. However, this equation is highly sensitive to the value of the impact threshold friction velocity and the observed agreement is greatly compromised for different values of  $u_{*,it}$ . Bagnold (1941) and Sørensen (2004) proposed expressions for  $Q$  proportional to  $u_*^3$ . When using the coefficients proposed by Vionnet et al. (2014), a greater mass flux is obtained with Sørensen's expression in comparison with the simulation results. Vionnet et al. (2014) estimated those coefficients from fitting  $Q_{S\emptyset}$  to the experimental measurements of Nishimura and Hunt (2000). Conversely, the expression proposed by Bagnold (1941) to describe saltation over uniform grains ( $C = 1.5$ ) predicts lower values for  $Q$ . For friction velocities lower than  $0.6 \text{ m s}^{-1}$ , the simulation results agree well with the model proposed by Bagnold (1941) if the constant parameter  $C$  is increased to 2.8. However, the curve obtained with  $C = 2.8$  is only expected to describe saltation over a bed of mixed-sized grains. The expression

proposed by Pomeroy and Gray (1990) underestimates the integrated mass flux in comparison with the remaining models and the simulation results. This is partly justified by the authors assumption of a relatively shallow saltation layer (saltation layer height varying from 0.7 to 5 cm for  $u_*$  varying from 0.3 to 0.8 m s<sup>-1</sup>). However, even by adjusting the height of integration from 15 cm to the proposed values, the integrated mass flux obtained with the current numerical model is significantly greater than the evolution proposed by Pomeroy and Gray (1990). Hence, the deviation between  $Q_{P&G}$  and the remaining models and simulation results is mainly related to the erroneous scaling of the integrated mass flux with  $u_*$ .

#### 4.2. The Effect of Mean Grain Diameter

In this section, we continue the analysis of saltation over a bed of equally sized grains. The effect of grain size is studied by comparing the results presented in the previous section (S1,  $\langle d \rangle = 200 \mu\text{m}$ ) with those from simulations S2, obtained for different grain sizes.

The vertical profiles of particle mass flux, concentration and mean streamwise velocity obtained for grain diameters ranging from 200 to 400  $\mu\text{m}$  are presented in Figures 2d–2f. It can be observed that particle streamwise velocity decreases when the grain size increases (Figure 2f). This is due to the fact that aerodynamic drag applied to the saltating particles increases approximately with  $d^2$ , but particle mass increases with  $d^3$ . Hence, the ability of the flow to accelerate the saltating grains reduces with particle mass. The near surface particle velocity also decreases with the grain diameter (inset in Figure 2f). Although the near surface particle velocity does not vary significantly with  $u_*$ , it clearly varies with the grain size.

As the grain size increases, the particle mass flux decreases near the surface and increases at higher elevations of the saltation layer (Figure 2d). Near the surface, this trend is justified by the decrease in particle streamwise velocity as  $\langle d \rangle$  increases (Figure 2f). Above  $\sim 4$  cm, the increase in particle mass flux as the grain size increases is due to the rise in particle concentration (Figure 2e), which is related to both an increase in particle mass and the number of particles aloft. The vertical profiles of particle mass flux obtained for  $u_* = 0.4 \text{ m s}^{-1}$  are also presented in logarithmic scale in Figure 7a. The results obtained with  $\langle d \rangle = 100 \mu\text{m}$  are added for comparison. An exponential decay along the saltation layer is clear for the greater grain sizes ( $\langle d \rangle$  between 200 and 400  $\mu\text{m}$ ), which is in agreement with field measurements (Martin & Kok, 2017) as previously discussed in Section 4.1. The vertical profile obtained with the smallest grain size ( $\langle d \rangle = 100 \mu\text{m}$ ) differs significantly from the others. A similar trend inside the saltation layer is visible up to 1 cm height. However, at greater heights, the profile assumes a different shape suggesting transition from saltation to suspension. In fact, for the smallest grain size, particles can be observed up to the top of the domain, while for greater grain sizes, aeolian transport seems to occur via saltation only as the mass flux ceases at approximately 14 cm height.

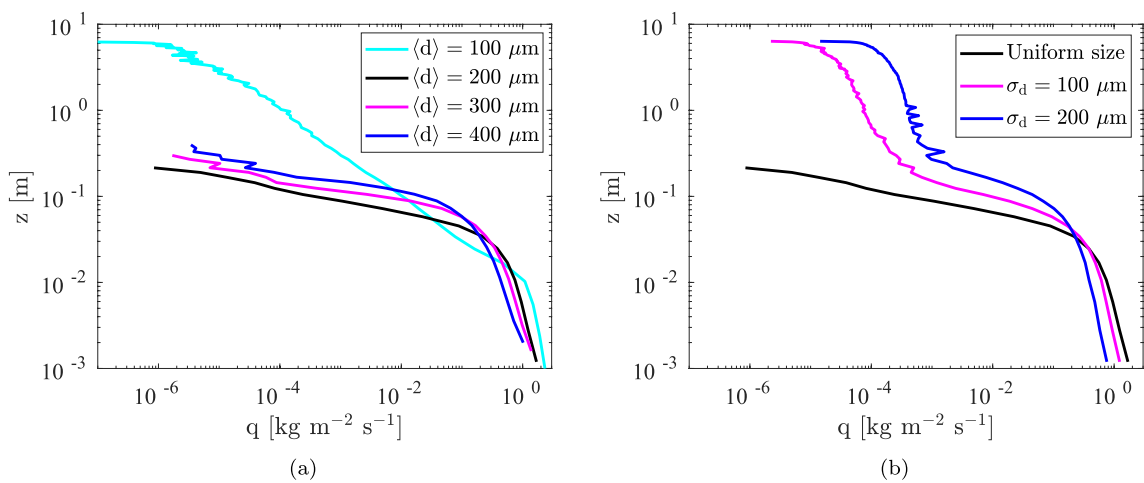


**Figure 7.** Vertical profiles of particle mass flux obtained with simulations S2 (a) and S3 (b) for  $u_* = 0.4 \text{ m s}^{-1}$ . Results from simulations S1 are presented for comparison.

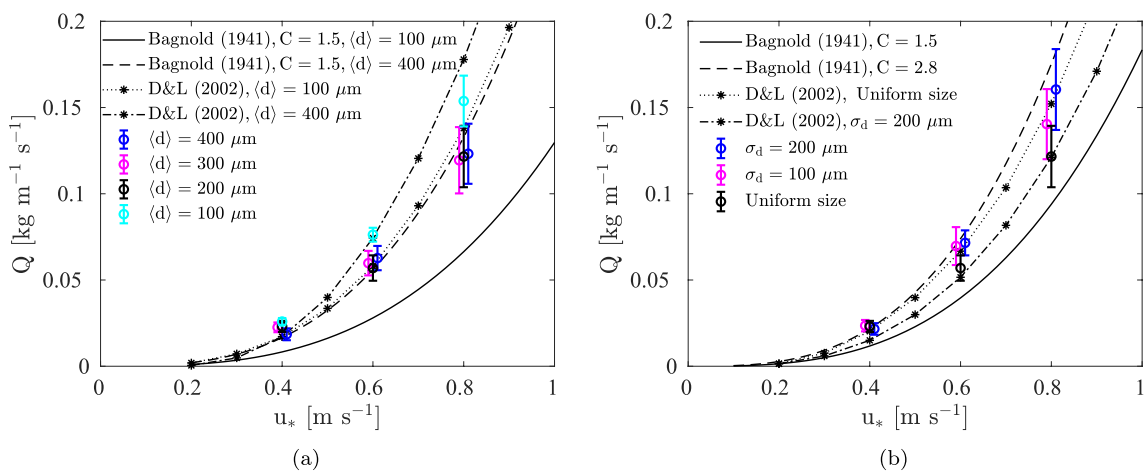


**Figure 8.** Integrated mass flux obtained with simulations S2 (a) and S3 (b) for  $u_*$  equal to 0.4, 0.6 and 0.8  $\text{m s}^{-1}$ . Results from simulations S1 obtained with the same  $u_*$  are also presented for comparison. To improve readability, some data points are slightly shifted in the  $u_*$  axis. The error bar is twice the standard deviation of the results. The curves are obtained from Bagnold's model ( $Q_{\text{Bag}}$  in Table 4) and from the numerical model proposed by Doorschot and Lehning (2002) (D&L). In (a), the curves are computed considering a uniform bed characterized by different grain diameters. In (b), both a uniform and a mixed-sized bed with a mean grain diameter of 200  $\mu\text{m}$  are considered.

The integrated mass flux is presented in Figure 8a along with the expression proposed by Bagnold (1941) and the numerical results from Doorschot and Lehning (2002) for varying mean grain diameters and friction velocities. Bagnold's expression establishes that  $Q$  is proportional to  $\langle d \rangle^{\frac{1}{2}}$ , following his wind tunnel experiments performed with uniform sand beds characterized by mean diameters ranging from 100  $\mu\text{m}$  to 1 mm. The numerical model of Doorschot and Lehning (2002) also predicts an increase in the integrated mass flux with the grain diameter. In contrast, a negligible variation is obtained with our model for grain diameters ranging from 200 to 400  $\mu\text{m}$ : the reduction in mass flux near the surface and its increase at higher elevations for increasingly bigger grains (Figure 2d) counterbalance each other. In fact, other saltation models do not predict an explicit variation of  $Q$  with particle mean diameter (e.g., Durán et al., 2011; Sørensen, 2004). In opposition to Bagnold's experiments, the wind tunnel measurements carried out by Dong et al. (2003) revealed a reduction in the integrated mass flux with the grain diameter. However, the comparison between sand beds is performed considering the same wind speed at a given reference height. Hence, it is observed that for the same wind speed at the chosen reference height, the integrated mass flux decreases as the grain size increases. In the simulations performed, the imposed friction velocity is kept constant when varying the grain size, which implies different velocities at a given reference height, depending on the mass flux of saltating particles and the respective momentum transfer. The negligible variation of the integrated mass flux with  $\langle d \rangle$  obtained with our model goes along with an increase in the wind speed at all heights as the grain size increases. When analyzing the experiments of Dong et al. (2003) performed with different grain sizes but yielding similar integrated mass fluxes, a greater wind speed is also obtained for greater grain sizes.

When considering a uniform bed with grains of 100  $\mu\text{m}$ , a greater integrated mass flux is obtained. However, as previously discussed, particles between 1 and 15 cm height might not be in saltation but rather in suspension. When modeling particles smaller than 200  $\mu\text{m}$ , a rigorous definition of the saltation layer height is needed to fully assess the impact of the mean diameter on the integrated mass flux in saltation.

The equilibrium surface friction velocity varies considerably with the mean grain size. In Figure 9a, an increase of  $u_{*,eq}$  is observed when  $\langle d \rangle$  increases for values greater than 200  $\mu\text{m}$ , which is consistent with the results of Kok and Renno (2009). For a given  $u_*$ , the total momentum transfer from the fluid to the particles decreases for greater grain diameters. This is partly due to a smaller number of particles aloft, which overcomes the increase in drag applied on each grain.

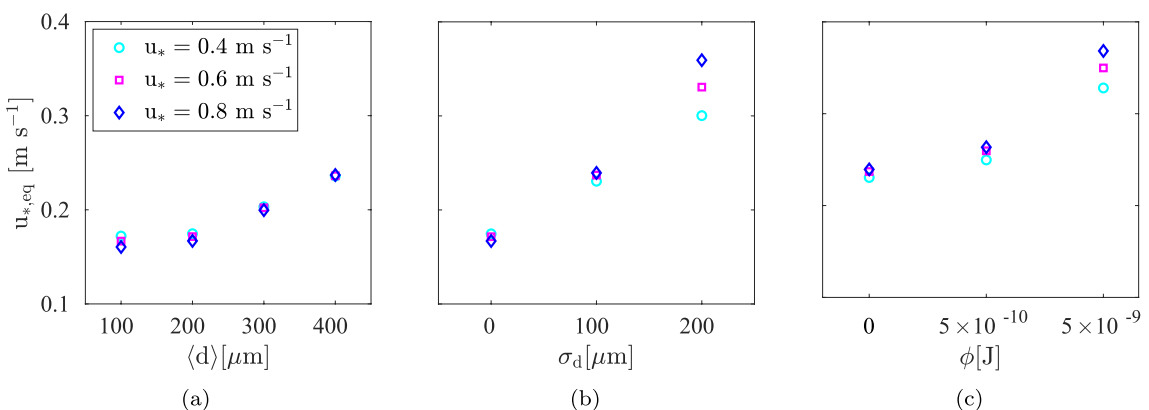


**Figure 9.** Equilibrium friction velocity obtained with simulations S2 (a), S3 (b) and S4 (c). In (a and b), results from simulations S1 are presented for comparison. In (c), results from simulations S3 are presented for comparison.

#### 4.3. The Effect of Mixed-Sized Grains

In order to model saltation over a bed of mixed-sized grains, the size distribution of surface grains is described by a lognormal distribution. In this section, the results from simulations S3, obtained with different standard deviations of the grain diameter, are presented and compared with those from simulations S1, obtained with a uniform grain size.

The vertical profiles of particle mass flux, concentration and mean streamwise velocity are presented in Figures 2g–2i. Grain size heterogeneity leads to a greater mean particle streamwise velocity, both near the surface and at higher elevations (Figure 2i). This is due to an increase in the number of smaller particles aloft, which are easily accelerated by the fluid flow. Similarly to Figure 2f (simulations S2), the variation of particle speed close to the surface with  $u_*$  is negligible; however, a clear variation with the bed characteristics is observed. The effect of the bed size distribution on the particle streamwise velocity profile is less significant when a mass-weighted average is considered. This is due to a reduced contribution of the smaller grains to the average profile.

Figures 2g and 2h show that grain size heterogeneity decreases particle mass flux and concentration close to the surface, but leads to greater values at higher elevations of the saltation layer. The vertical profiles of particle mass flux obtained for  $u_* = 0.4$  m s<sup>-1</sup> are presented in logarithmic scale in Figure 7b. As expected, close to the surface, an exponential decay across the saltation layer is observed. At higher elevations, a cloud of suspended grains forms above the saltation layer of mixed-sized beds and a second distinct exponential decay of the mass flux along the height is observed. The transition from saltation to suspension occurs between 5 and 12 cm height, approximately, and is characterized by the change in gradient of the mass flux profiles. This trend was previously observed in field measurements (Gordon et al., 2009) and other numerical models (e.g., Nemoto & Nishimura, 2004).

The probability density function (PDF) of particle size at different heights is presented in Figure 10 for  $u_* = 0.4$  m s<sup>-1</sup> and both size distributions ( $\sigma_d$  of 100 and 200 μm). The PDF of particle size at the bed is also presented for comparison (the left tail of the distribution is not obtained, as a minimum grain size of 50 μm is specified in the simulations). Below ~3 cm height, the size distribution of particles aloft is reasonably well approximated by a lognormal distribution. It is similar to the PDF at the bed, but skewed toward smaller grain sizes. From 5 to 10 cm height, a bi-lognormal distribution is visible in both simulations. In this region, for progressively greater heights, the probability density of smaller grains increases and the probability density of bigger grains decreases. Finally, above ~14 cm, a new lognormal distribution arises, characterized by grains smaller than 100 μm. The presented variation of particle size distribution with height agrees well with the results of Nemoto and Nishimura (2004) and is related to the saltation-suspension transition observed in Figure 7b. In drifting snow events, particle sublimation can change the size distribution by reducing the size of particles aloft. This modifies the equilibrium saltation state and enhances the transport of particles in suspension.

Figure 10b shows that a wider lognormal bed size distribution leads to smaller grain sizes in the first centimeters above the surface. Smaller grains and less particles aloft justify the decrease in mass flux close to the surface

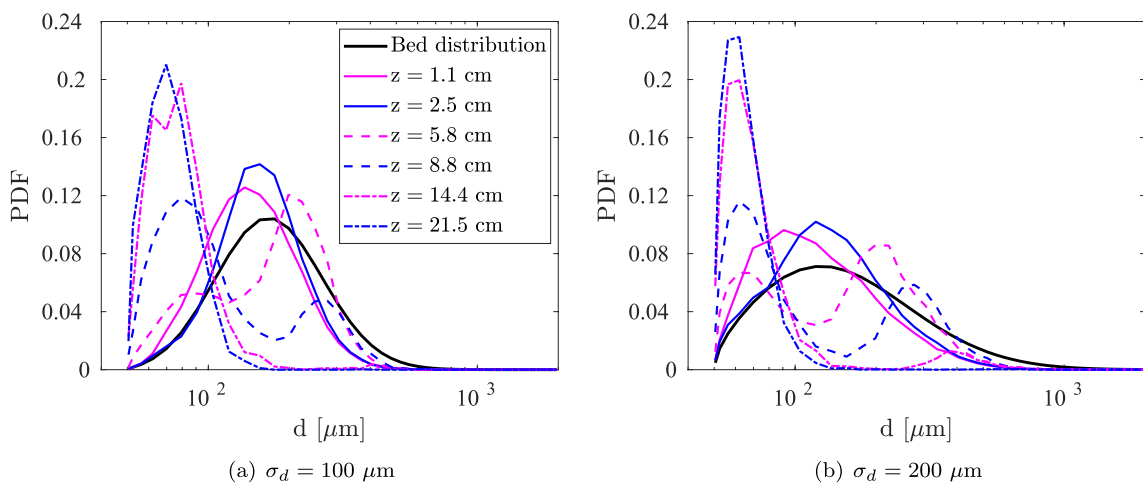


**Figure 10.** Probability density function (PDF) of particle size at the bed and at different heights obtained from simulations S3 considering  $u_* = 0.4 \text{ m s}^{-1}$ .

observed in Figure 7b. Moreover, the fraction of grains within the range 200–500  $\mu\text{m}$  present between 8 and 15 cm height is greater. Considering that these particles are transported in saltation, this is in agreement with the increase in saltation layer height observed in Figure 7b.

The integrated mass flux is presented in Figure 8b. The simulation results are compared with Bagnold's model, considering different values for the parameter  $C$  (Bagnold, 1941), and with the results of the numerical model proposed by Doorschot and Lehning (2002). In the latter, particle size is assumed uniform ( $\langle d \rangle = 200 \mu\text{m}$ ) or defined by a lognormal distribution ( $\langle d \rangle = 200 \mu\text{m}$ ,  $\sigma_d = 200 \mu\text{m}$ ). In general, the integrated mass flux obtained with the current model increases with bed heterogeneity. This trend is also predicted by Bagnold (1941). However, it contrasts with the evolution obtained with the model of Doorschot and Lehning (2002), in which  $Q$  decreases when the bed heterogeneity increases. The effect of bed size distribution on the integrated mass flux underlines the importance of correctly describing particle size when estimating snow saltation mass flux. According to the simulation results, this is particularly relevant when  $u_*$  is greater than  $0.4 \text{ m s}^{-1}$ . Even though a rigorous definition of the saltation layer height is not taken in this work, similar trends are obtained when the integration height is limited to the first 10 cm. Moreover, the effect of bed heterogeneity on the computed integrated mass flux is even more significant if the suspension layer is taken into account. The integrated mass flux obtained for a uniform bed of grains with  $100 \mu\text{m}$  in diameter is closer to the values obtained for the studied mixed-sized beds, compared to the other uniform beds with larger grains (Figure 8a). However, over the uniform bed with grains of  $100 \mu\text{m}$ , particles above 1 cm height seem to be transported in suspension (Figure 7a). Taking also into account that an increase in the mean particle diameter from 200 to 400  $\mu\text{m}$  leads to a negligible variation of  $Q$  (Figure 8a), it is in general not possible to correctly model saltation over a mixed-size bed considering a representative diameter and equally sized grains.

An increase in bed heterogeneity also leads to an increase in the equilibrium surface friction velocity,  $u_{*,eq}$  (Figure 9b). In contrast with the simulations performed over equally sized grains,  $u_{*,eq}$  slightly increases with  $u_*$ . This trend is specially visible for the results obtained with  $\sigma_d = 200 \mu\text{m}$ . For a given  $u_*$ , the total exchange of momentum from the fluid to the particles decreases for greater standard deviations of the size distribution. Taking into account that the drag applied on each grain is approximately proportional to  $d^2$  and that the number of particles aloft does not vary in a monotonous way with  $\sigma_d$ , the decrease in the momentum exchange is explained by the presence of particles with diameters smaller than the mean value ( $\langle d \rangle = 200 \mu\text{m}$ ).

#### 4.4. The Effect of Interparticle Cohesion

We complete the analysis of mixed-sized bed saltation by studying the effect of interparticle cohesion. In this section, the results obtained with simulations S4 are presented. A bed of mixed-sized grains characterized by a log-normal distribution with  $\langle d \rangle = 200 \mu\text{m}$  and  $\sigma_d = 100 \mu\text{m}$  is considered. The results are compared with those from simulation S3, that were performed with the same particle size distribution but neglecting interparticle cohesion.

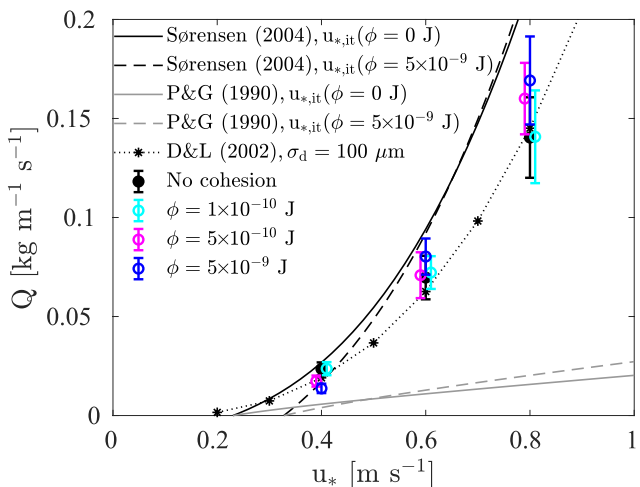


**Figure 11.** Integrated mass flux obtained with simulations S4 for  $u_*$  equal to 0.4, 0.6 and 0.8  $\text{m s}^{-1}$ . Results from simulations S3 obtained with the same size distribution and  $u_*$  are also presented for comparison. To improve readability, some data points are slightly shifted in the  $u_*$  axis. The error bar is twice the standard deviation of the results. The expressions proposed by Sørensen (2004) and Pomeroy and Gray (1990) (P&G) are plotted for comparison considering different values of the impact threshold friction velocity. The results from Doorschot and Lehning (2002) (D&L) are obtained for a bed characterized by a lognormal distribution with  $\langle d \rangle = 200 \mu\text{m}$  and  $\sigma_d = 100 \mu\text{m}$ .

this leads to a global decrease of particles aloft (Figure 2k). As a result, for greater values of cohesion energy, the total momentum transfer from the fluid to the particles is smaller (Figure 9c), as well as the consequent decrease in streamwise wind speed. This leads to a general increase in particle speed (Figure 2l). The initial velocity at which the splashed grains are ejected from the bed does not vary directly with interparticle cohesion (see distribution characteristics presented in Table 1). However, greater impact velocities lead to higher ejection velocities.

The integrated mass flux is presented in Figure 11. The results obtained with the saltation models proposed by Pomeroy and Gray (1990), Doorschot and Lehning (2002) and Sørensen (2004) are also presented for comparison. These models are currently used in atmospheric models, such as RACMO (Lenaerts et al., 2012), MAR (Amory et al., 2015, 2021), Alpine3D (Lehning et al., 2008) and Meso-NH (Vionnet et al., 2014), to estimate snow saltation mass flux. The expressions proposed by Pomeroy and Gray (1990) and Sørensen (2004) are plotted for two limiting values of the impact threshold friction velocity: obtained with simulation S3,  $\sigma_d = 100 \mu\text{m}$  (non-cohesive bed) and with simulation S4,  $\phi = 5 \times 10^{-9} \text{ J}$ . As previously explained, in this work, the impact threshold friction velocity is assumed equal to the equilibrium friction velocity at the lowest value of  $u_*$  that was studied ( $u_* = 0.4 \text{ m s}^{-1}$ ). The results obtained with the model developed by Doorschot and Lehning (2002) are derived considering a lognormal bed size distribution with  $\langle d \rangle = 200 \mu\text{m}$  and  $\sigma_d = 100 \mu\text{m}$ .

The simulation results indicate that  $Q$  varies significantly with the cohesion energy. In general, it decreases with  $\phi$  for lower friction velocities and increases with  $\phi$  for greater values of  $u_*$ . This is due to the reduction of particle mass flux close to the surface and to its increase at higher elevations as cohesion energy increases (Figure 2j). At low friction velocities ( $u_* = 0.4 \text{ m s}^{-1}$ ), the reduction of particle mass flux close to the surface (due to the decrease in particle concentration) prevails, while at greater  $u_*$ , the rise in mass flux at higher elevations (due to the increase in particle velocity) becomes more significant, leading to a global growth of the integrated mass flux. Naturally, for very high values of cohesion energy, for which particle ejection is highly compromised, the reduction in particle concentration is expected to prevail at all friction velocities, leading to a reduction in the integrated mass flux.

A better agreement between the expression proposed by Sørensen (2004), using the parameters proposed by Vionnet et al. (2014), and the simulation results is obtained when interparticle cohesion and a lognormal size

The vertical profiles of particle mass flux, concentration and mean streamwise velocity are presented in Figures 2j–2l. As cohesion energy increases, particle concentration decreases significantly close to the surface and increases slightly at higher regions of the saltation layer (Figure 2k). Particle mean streamwise velocity increases with cohesion energy at all heights (Figure 2l). As expected, close to the surface, a negligible variation of particle streamwise velocity is obtained for different  $u_*$ ; however, a clear variation with interparticle cohesion is seen. As the ejection velocity increases, the maximum height attained by the saltating particles increases as well. This justifies the observed larger particle concentration at higher elevations. Particle mass flux is given by the product of particle concentration and streamwise velocity. It decreases close to the surface due to a strong reduction in the number of particles and increases at higher regions of the saltation layer due to the rise of both the number of particles aloft and the particle streamwise velocity (Figure 2j).

The equilibrium friction velocity,  $u_{*,eq}$ , is presented in Figure 9c. It is expected to vary with the bed type, and therefore, with the strength of the interparticle bonds. In fact,  $u_{*,eq}$  increases with the cohesion energy, which was also obtained by Comola, Gaume, et al. (2019).

Cohesion energy has a direct effect on the number of ejected grains computed from energy conservation,  $N_E$  (see Equation 8a). If  $N_E$  becomes smaller than  $N_M$ , the number of ejected grains is restricted by energy conservation and it decreases for increasing values of  $\phi$ . Hence, for the same impact velocity and impacting grain diameter, the number of splashed grains reduces with cohesion energy (Comola & Lehning, 2017). Our results suggest that

the simulation results indicate that  $Q$  varies significantly with the cohesion energy. In general, it decreases with  $\phi$  for lower friction velocities and increases with  $\phi$  for greater values of  $u_*$ . This is due to the reduction of particle mass flux close to the surface and to its increase at higher elevations as cohesion energy increases (Figure 2j). At low friction velocities ( $u_* = 0.4 \text{ m s}^{-1}$ ), the reduction of particle mass flux close to the surface (due to the decrease in particle concentration) prevails, while at greater  $u_*$ , the rise in mass flux at higher elevations (due to the increase in particle velocity) becomes more significant, leading to a global growth of the integrated mass flux. Naturally, for very high values of cohesion energy, for which particle ejection is highly compromised, the reduction in particle concentration is expected to prevail at all friction velocities, leading to a reduction in the integrated mass flux.

distribution are considered. This is, when considering a more realistic snow bed. Nonetheless, greater values for  $Q$  are predicted with  $Q_{S\phi}$ . An overestimation of the integrated mass flux in saltation is consistent with the overestimation of blowing snow particles obtained by Vionnet et al. (2014, 2017). The effect of the impact threshold friction velocity on  $Q_{S\phi}$  is mainly visible at lower friction velocities. At  $u_* = 0.4 \text{ m s}^{-1}$ , the adjustment of the impact threshold friction velocity improves the agreement between model and simulation results obtained with different values for cohesion energy. The results obtained with the numerical model of Doorschot and Lehning (2002) agree well with the simulation results obtained with mixed-sized and cohesionless grains or  $\phi = 10^{-10} \text{ J}$ , over the whole range of the studied friction velocities. Even though a good agreement is also obtained over a bed of uniform grains for  $u_* < 0.6 \text{ m s}^{-1}$  (Figure 6b), the effect of mean grain diameter and bed heterogeneity on the integrated mass flux predicted by Doorschot and Lehning (2002) is not consistent with the evolution obtained by the present model (Figure 8). The expression proposed by Pomeroy and Gray (1990) considerably underestimates the integrated mass flux in comparison with the simulation results and remaining models, independently of the assumed values for the impact threshold friction velocity. The underestimation of the saltation mass flux might be one of the causes for the underestimation of the blowing snow mass flux obtained by Amory et al. (2015).

In the drifting snow model proposed by Amory et al. (2021), the integrated mass flux in saltation is also computed with the expression of Pomeroy and Gray (1990). However, more reasonable estimates of the blowing snow mass flux are obtained. This is mainly attributed to the improved calculation of the fluid threshold friction velocity and of snow densification induced by the occurrence of drifting snow. Other aspects of the drifting snow model will also influence the particle mass flux in suspension near the surface. They are, for example, the type of lower boundary condition implemented, the turbulence diffusivity considered in the saltation-suspension transition region, and the assumed particle streamwise velocity above the saltation layer.

## 5. Conclusions

The modeling of snow saltation is particularly challenging due to the metamorphic nature of snow. Depending on the meteorological conditions, snow grains can have multiple shapes and sizes and form interparticle ice bonds between them. During snow transport, the interparticle bonds break and snow particles shape and size change due to fragmentation and sublimation. However, snow saltation models used in mesoscale models generally neglect or oversimplify these particularities, leading to uncertainties in the estimated mass flux that are difficult to quantify. In this work, an LES-based model coupled with state-of-the-art splash functions is used to simulate the complex particle-wind-bed interactions. This approach allows the modeling of steady state saltation over a variety of bed types and the analysis of the effect of grain size and interparticle cohesion on saltation dynamics.

The numerical model is able to simulate the main saltation characteristics observed in previous models and experiments: the focus point in the average streamwise wind profiles, an average streamwise particle speed close to the surface invariant with respect to the friction velocity, the exponential decay of particle mass flux with increasing height, and the scaling of the integrated mass flux with the square of the friction velocity. Moreover, as expected, for friction velocities sufficiently greater than the fluid threshold friction velocity, the resulting steady state is characterized by a dynamic equilibrium between splash and deposition. Over mixed-sized beds, different particle size distributions are obtained depending on the distance to the snow surface, as expected when transition from saltation to suspension occurs.

The relative importance of snow bed characteristics on saltation dynamics is analyzed by varying the particle size distribution and interparticle bond strength in a systematic way. Bed characteristics, as grain size and interparticle cohesion, significantly influence saltation dynamics, in particular, particle speed, surface friction velocity and integrated mass flux. Particle speed close to the surface is approximately invariant with respect to the friction velocity for all beds that were considered; however, it varies with the bed type. This is relevant for the development of simple saltation models, which are usually based on an assumption for the near surface particle speed. Nevertheless, the mean particle speed in the saltation layer increases with the friction velocity. The average surface friction velocity during steady state saltation, defined here as the equilibrium friction velocity, increases for greater values of the mean grain diameter, standard deviation of the size distribution and interparticle cohesion. The equilibrium friction velocity is tightly correlated with the impact threshold friction velocity, which is an important parameter to estimate saltation mass flux. Over uniform beds, a negligible variation of the integrated mass

flux with particle size is obtained for particles ranging between 200 and 400  $\mu\text{m}$ . When considering a mixed-sized bed characterized by a lognormal distribution, an increase in the integrated mass flux is seen due to an average increase in particle speed and concentration. The results presented highlight that the integrated mass flux over mixed-sized beds can be hardly reproduced by an equally sized bed with a representative mean diameter - a tempting assumption in simple saltation models. The integrated mass flux also varies with interparticle cohesion, but in a non-monotonous way: it decreases with the strength of interparticle bonds for lower friction velocities and it increases for higher friction velocities. Overall, greater values of cohesion lead to a reduction in the number of particles aloft which, at high wind speeds, is balanced by an increase in particle speed. In general, the greater the friction velocity, the greater the effect of bed properties on saltation characteristics. High wind speed events might be rare in some regions. However, they are responsible for major modifications of the snow cover.

The agreement between simulation results and the saltation models typically used in large scale atmospheric models depends on the bed characteristics. For specific bed types, a relatively good agreement with the computed integrated mass flux can be obtained with the models of Sørensen (2004), using the parameters proposed by Vionnet et al. (2014), and Doorschot and Lehning (2002). However, these models either consider fixed parameters, which are not adjustable to the snow type, or predict a different variation of the integrated mass flux with the mean grain size and bed heterogeneity. A systematic underestimation and overestimation of the integrated mass flux is obtained with the expression proposed by Pomeroy and Gray (1990) and Sørensen (2004), respectively. This might partly justify the underestimation and overestimation of blowing snow mass flux presented, respectively, by Amory et al. (2015) and Vionnet et al. (2014, 2017). Inaccuracies in the calculation of particle concentration at the top of the saltation layer can also be related to poor estimates of the vertical profile of particle mass flux, the averaged streamwise particle speed and the saltation layer height. Grain size and interparticle cohesion influence all variables of interest. Therefore, improvements on snow transport models can only be reached if all the referred quantities are correctly represented.

Further efforts must be made to fully model the effect of bed characteristics on snow saltation. For example, interparticle cohesion is also expected to influence particle ejection velocity during splash and the fluid threshold for the onset of aerodynamic entrainment (Comola et al., 2021). Moreover, the strength of interparticle bonds between grains that did not leave the surface and between those that failed to rebound might not be the same. From the experimental work side, a correlation between interparticle cohesion and meteorological conditions or measurable snow properties like snow density or snow hardness is still needed. In addition, exhaustive direct comparisons between simulation results and experimental measurements of snow saltation must be performed to complete model validation. In order to better assess the model inner parameters, further studies of the splash process over natural snow beds are required, as well as detailed field measurements characterizing both the wind speed, the snow bed and the particles in saltation.

Simple and computationally inexpensive saltation models are much needed in mesoscale models. However, the in depth study of snow saltation is necessary to fully understand the implications of the simplifying assumptions that are used and to estimate the errors they might introduce. This article shows the capabilities of an LES-based model to simulate snow saltation, presents the effect of bed properties on saltation dynamics and motivates further studies in this field. It highlights the limitations of the snow saltation models currently employed in atmospheric models and the need for improved ones that take into account the effect of snow surface characteristics. Without accurate estimations for the mass flux in saltation, atmospheric models will hardly deliver reasonable estimates of blowing snow mass flux and sublimation. Hence, the effect of snow transport and sublimation on large scale mass and energy balances is highly compromised.

## Data Availability Statement

The source code and the simulation results presented in the figures are available at <https://www.envidat.ch/#/metadata/modeling-snow-saltation-the-effect-of-grain-size-and-interparticle-cohesion>

## Acknowledgments

The authors acknowledge the contribution of three anonymous reviewers for their valuable and constructive comments. Pedro Cabral is acknowledged for the numerous discussions regarding the results and the in-depth revision of the text. His contribution has greatly improved the clarity of the manuscript. The authors acknowledge the Swiss National Science Foundation (SNSF) for the financial support (projects number 179130 and P2ELP2\_178219) and the Swiss National Supercomputing Centre (CSCS) for providing the computational resources (projects s873, s938 and s1031). Open access funding provided by Ecole Polytechnique Federale de Lausanne.

## References

- Agosta, C., Amory, C., Kittel, C., Orsi, A., Favier, V., Gallée, H., et al. (2019). Estimation of the Antarctic surface mass balance using the regional climate model MAR (1979–2015) and identification of dominant processes. *The Cryosphere*, 13(1), 281–296. <https://doi.org/10.5194/tc-13-281-2019>
- Aksamit, N. O., & Pomeroy, J. W. (2016). Near-surface snow particle dynamics from particle tracking velocimetry and turbulence measurements during alpine blowing snow storms. *The Cryosphere*, 10(6), 3043–3062. <https://doi.org/10.5194/tc-10-3043-2016>
- Aksamit, N. O., & Pomeroy, J. W. (2018). Scale interactions in turbulence for mountain blowing snow. *Journal of Hydrometeorology*, 19(2), 305–320. <https://doi.org/10.1175/jhm-d-17-0179.1>
- Albertson, J. D., & Parlange, M. B. (1999). Natural integration of scalar fluxes from complex terrain. *Advances in Water Resources*, 23, 239–252. [https://doi.org/10.1016/s0309-1708\(99\)00011-1](https://doi.org/10.1016/s0309-1708(99)00011-1)
- Almeida, M. P., Andrade, J. S., & Herrmann, H. J. (2006). Aeolian transport layer. *Physical Review Letters*, 96(1), 018001. <https://doi.org/10.1103/physrevlett.96.018001>
- Ammi, M., Oger, L., Beladjine, D., & Valance, A. (2009). Three-dimensional analysis of the collision process of a bead on a granular packing. *Physical Review E - Statistical, Nonlinear and Soft Matter Physics*, 79, 021305. <https://doi.org/10.1103/physreve.79.021305>
- Amory, C., Kittel, C., Le Toumelin, L., Agosta, C., Delhasse, A., Favier, V., & Fettweis, X. (2021). Performance of MAR (v3.11) in simulating the drifting-snow climate and surface mass balance of Adélie Land, East Antarctica. *Geoscientific Model Development*, 14(6), 3487–3510. <https://doi.org/10.5194/gmd-14-3487-2021>
- Amory, C., Trouvilliez, A., Gallée, H., Favier, V., Naaim-Bouvet, F., Gentron, C., et al. (2015). Comparison between observed and simulated aeolian snow mass fluxes in Adélie Land, East Antarctica. *The Cryosphere*, 9(4), 1373–1383. <https://doi.org/10.5194/tc-9-1373-2015>
- Anderson, R. S., & Haff, P. K. (1988). Simulation of Eolian Saltation. *Science*, 241(4867), 820–823. <https://doi.org/10.1126/science.241.4867.820>
- Anderson, R. S., & Haff, P. K. (1991). Wind modification and bed response during saltation of sand in air. In O. E. Barndorff-Nielsen, & B. B. Willets (Eds.), *Aeolian grain transport 1* (pp. 21–51). Springer Vienna. [https://doi.org/10.1007/978-3-7091-6706-9\\_2](https://doi.org/10.1007/978-3-7091-6706-9_2)
- Anderson, R. S., & Hallet, B. (1986). Sediment transport by wind: Toward a general model. *GSA Bulletin*, 97(5), 523–535. [https://doi.org/10.1130/0016-7606\(1986\)97<523:STBWT>2.0.CO;2](https://doi.org/10.1130/0016-7606(1986)97<523:STBWT>2.0.CO;2)
- Araoka, K., & Maeno, N. (1981). Dynamical behaviors of snow particles in the saltation layer. In *Proceedings of the third symposium on polar meteorology and glaciology* (Vol. 19, pp. 253–263). Memoirs of National Institute of Polar Research. Tokyo.
- Bagnold, R. A. (1941). *The physics of blown sand and desert dunes*. Dover Publications.
- Bou-Zeid, E., Meneveau, C., & Parlange, M. (2005). A scale-dependent Lagrangian dynamic model for large eddy simulation of complex turbulent flows. *Physics of Fluids*, 17(2), 025105. <https://doi.org/10.1063/1.1839152>
- Canuto, C., Hussaini, M. Y., Quarteroni, A., & Zang, T. A. (1988). *Spectral Methods in Fluid Dynamics*. Springer-Verlag Berlin Heidelberg.
- Chepil, W. S. (1959). Equilibrium of Soil Grains at the Threshold of Movement by Wind. *Soil Science Society of America*, 23(6), 422–428. <https://doi.org/10.2136/sssaj1959.03615995002300060019x>
- Clifton, A., & Lehning, M. (2008). Improvement and validation of a snow saltation model using wind tunnel measurements. *Earth Surface Processes and Landforms*, 33(14), 2156–2173. <https://doi.org/10.1002/esp.1673>
- Clifton, A., Rüedi, J.-D., & Lehning, M. (2006). Snow saltation threshold measurements in a drifting-snow wind tunnel. *Journal of Glaciology*, 52(179), 585–596. <https://doi.org/10.3189/172756506781828430>
- Colbeck, S. (1986). Statistics of coarsening in water-saturated snow. *Acta Metallurgica*, 34(3), 347–352. [https://doi.org/10.1016/0001-6160\(86\)90070-2](https://doi.org/10.1016/0001-6160(86)90070-2)
- Comola, F. (2017). *Stochastic modeling of snow transport and hydrologic response in alpine terrain* (PhD thesis). Ecole Polytechnique Fédérale de Lausanne, Lausanne, Switzerland.
- Comola, F., Gaume, J., Kok, J. F., & Lehning, M. (2019). Cohesion-induced enhancement of aeolian saltation. *Geophysical Research Letters*, 46, 5566–5574. <https://doi.org/10.1029/2019gl082195>
- Comola, F., Giometto, M. G., Salesky, S. T., Parlange, M. B., & Lehning, M. (2019). Preferential deposition of snow and dust over hills: Governing processes and relevant scales. *Journal of Geophysical Research: Atmospheres*, 124, 7951–7974. <https://doi.org/10.1029/2018jd029614>
- Comola, F., Kok, J. F., Gaume, J., Paterna, E., & Lehning, M. (2017). Fragmentation of wind-blown snow crystals. *Geophysical Research Letters*, 44, 4195–4203. <https://doi.org/10.1002/2017gl073039>
- Comola, F., Kok, J. F., Lora, J. M., Cohenim, K., Yu, X., He, C., et al. (2021). Intermittent saltation drives Mars-like aeolian activity on Titan. *EarthArXiv*. <https://doi.org/10.31223/X52G7H>
- Comola, F., & Lehning, M. (2017). Energy- and momentum-conserving model of splash entrainment in sand and snow saltation. *Geophysical Research Letters*, 44, 1601–1609. <https://doi.org/10.1002/2016gl071822>
- Crivelli, P., Paterna, E., Horender, S., & Lehning, M. (2016). Quantifying particle numbers and mass flux in drifting snow. *Boundary-Layer Meteorology*, 161(3), 519–542. <https://doi.org/10.1007/s10546-016-0170-9>
- Déry, S. J., & Yau, M. K. (1999). A bulk blowing snow model. *Boundary-Layer Meteorology*, 93(2), 237–251. <https://doi.org/10.1023/a:100206515856>
- Diebold, M., Higgins, C., Fang, J., Bechmann, A., & Parlange, M. B. (2013). Flow over Hills: A large-eddy simulation of the bulund case. *Boundary-Layer Meteorology*, 148(1), 177–194. <https://doi.org/10.1007/s10546-013-9807-0>
- Dietrich, W. E. (1982). Settling velocity of natural particles. *Water Resources Research*, 18, 1615–1626. <https://doi.org/10.1029/wr018i006p01615>
- Dong, Z., Liu, X., Wang, H., & Wang, X. (2003). Aeolian sand transport: A wind tunnel model. *Sedimentary Geology*, 161(1), 71–83. [https://doi.org/10.1016/s0037-0738\(02\)00396-2](https://doi.org/10.1016/s0037-0738(02)00396-2)
- Doorschot, J., & Lehning, M. (2002). Equilibrium saltation: Mass fluxes, aerodynamic entrainment, and dependence on grain properties. *Boundary-Layer Meteorology*, 104(1), 111–130. <https://doi.org/10.1023/a:1015516420286>
- Doorschot, J., Lehning, M., & Vrouwe, A. (2004). Field measurements of snow-drift threshold and mass fluxes, and related model simulations. *Boundary-Layer Meteorology*, 113(3), 347–368. <https://doi.org/10.1007/s10546-004-8659-z>
- Dupont, S., Bergametti, G., Marticorena, B., & Simoëns, S. (2013). Modeling saltation intermittency. *Journal of Geophysical Research: Atmospheres*, 118, 7109–7128. <https://doi.org/10.1002/jgrd.50528>
- Durán, O., Andreotti, B., & Claudin, P. (2012). Numerical simulation of turbulent sediment transport, from bed load to saltation. *Physics of Fluids*, 24(10), 103306. <https://doi.org/10.1063/1.4757662>
- Durán, O., Claudin, P., & Andreotti, B. (2011). On aeolian transport: Grain-scale interactions, dynamical mechanisms and scaling laws. *Aeolian Research*, 3(3), 243–270. <https://doi.org/10.1016/j.aeolia.2011.07.006>
- Fierz, C., Armstrong, R. L., Durand, Y., Etchevers, P., Greene, E., McClung, D. M., & Sokratov, S. A. (2009). The international classification for seasonal snow on the ground. In *IHP-VII Technical Documents in Hydrology*, No 83, IACS contribution No 1. UNESCO-IHP.

- Gauer, P. (2001). Numerical modeling of blowing and drifting snow in Alpine terrain. *Journal of Glaciology*, 47(156), 97–110. <https://doi.org/10.3189/172756501781832476>
- Giometto, M. G., Christen, A., Egli, P. E., Schmid, M. F., Tooke, R. T., Coops, N. C., & Parlange, M. B. (2017). Effects of trees on mean wind, turbulence and momentum exchange within and above a real urban environment. *Advances in Water Resources*, 106, 154–168. <https://doi.org/10.1016/j.advwatres.2017.06.018>
- Giometto, M. G., Christen, A., Meneveau, C., Fang, J., Krafczyk, M., & Parlange, M. B. (2016). Spatial characteristics of roughness sub-layer mean flow and turbulence over a realistic urban surface. *Boundary-Layer Meteorology*, 160(3), 425–452. <https://doi.org/10.1007/s10546-016-0157-6>
- Gordon, M., Savelyev, S., & Taylor, P. A. (2009). Measurements of blowing snow, part II: Mass and number density profiles and saltation height at Franklin Bay, NWT, Canada. *Cold Regions Science and Technology*, 55(1), 75–85. <https://doi.org/10.1016/j.coldregions.2008.07.001>
- Gromke, C., Horender, S., Walter, B., & Lehning, M. (2014). Snow particle characteristics in the saltation layer. *Journal of Glaciology*, 60(221), 431–439. <https://doi.org/10.3189/2014jog13j079>
- Groot Zwaaftink, C. D., Diebold, M., Horender, S., Overney, J., Lieberherr, G., Parlange, M. B., & Lehning, M. (2014). Modelling small-scale drifting snow with a lagrangian stochastic model based on large-eddy simulations. *Boundary-Layer Meteorology*, 153(1), 117–139. <https://doi.org/10.1007/s10546-014-9934-2>
- Guala, M., Manes, C., Clifton, A., & Lehning, M. (2008). On the saltation of fresh snow in a wind tunnel: Profile characterization and single particle statistics. *Journal of Geophysical Research*, 113. <https://doi.org/10.1029/2007jf000975>
- Ho, T. D., Valance, A., Dupont, P., & Ould El Moctar, A. (2011). Scaling laws in aeolian sand transport. *Physical Review Letters*, 106(9), 094501. <https://doi.org/10.1103/physrevlett.106.094501>
- Huang, N., Zhang, Y., & D'Adamo, R. (2007). A model of the trajectories and midair collision probabilities of sand particles in a steady state saltation cloud. *Journal of Geophysical Research*, 112. <https://doi.org/10.1029/2006jd007480>
- Kok, J. F., Parteli, E. J. R., Michaels, T. I., & Karam, D. B. (2012). The physics of wind-blown sand and dust. *Reports on Progress in Physics*, 75(10), 106901. <https://doi.org/10.1088/0034-4885/75/10/106901>
- Kok, J. F., & Renno, N. O. (2006). Enhancement of the emission of mineral dust aerosols by electric forces. *Geophysical Research Letters*, 33. <https://doi.org/10.1029/2006gl026284>
- Kok, J. F., & Renno, N. O. (2008). Electrostatics in wind-blown sand. *Physical Review Letters*, 100(1), 014501. <https://doi.org/10.1103/physrevlett.100.014501>
- Kok, J. F., & Renno, N. O. (2009). A comprehensive numerical model of steady state saltation (COMSALT). *Journal of Geophysical Research*, 114. <https://doi.org/10.1029/2009jd011702>
- Lämmel, M., Dzikowski, K., Kroy, K., Oger, L., & Valance, A. (2017). Grain-scale modeling and splash parametrization for aeolian sand transport. *Physical Review E*, 95(2), 022902. <https://doi.org/10.1103/physreve.95.022902>
- Lehning, M., Doorschot, J., & Bartelt, P. (2000). A snowdrift index based on SNOWPACK model calculations. *Annals of Glaciology*, 31, 382–386. <https://doi.org/10.3189/172756400781819770>
- Lehning, M., Löwe, H., Ryser, M., & Raderschall, N. (2008). Inhomogeneous precipitation distribution and snow transport in steep terrain. *Water Resources Research*, 44(7). <https://doi.org/10.1029/2007wr006545>
- Lenaeerts, J. T. M., van den Broeke, M. R., Déry, S. J., van Meijgaard, E., van de Berg, W. J., Palm, S. P., & Sanz Rodrigo, J. (2012). Modeling drifting snow in Antarctica with a regional climate model: 1. Methods and model evaluation. *Journal of Geophysical Research*, 117. <https://doi.org/10.1029/2011jd016145>
- Martin, R. L., & Kok, J. F. (2017). Wind-invariant saltation heights imply linear scaling of aeolian saltation flux with shear stress. *Science Advances*, 3(6), e1602569. <https://doi.org/10.1126/sciadv.1602569>
- Maxey, M. R., & Riley, J. J. (1983). Equation of motion for a small rigid sphere in a nonuniform flow. *The Physics of Fluids*, 26(4), 883–889. <https://doi.org/10.1063/1.864230>
- McEwan, I. K., & Willetts, B. B. (1991). Numerical model of the saltation cloud. In O. E. Barndorff-Nielsen, & B. B. Willetts (Eds.), *Aeolian grain transport 1* (pp. 53–66). Springer Vienna. [https://doi.org/10.1007/978-3-7091-6706-9\\_3](https://doi.org/10.1007/978-3-7091-6706-9_3)
- Munters, W., Meneveau, C., & Meyers, J. (2016). Shifted periodic boundary conditions for simulations of wall-bounded turbulent flows. *Physics of Fluids*, 28(2), 025112. <https://doi.org/10.1063/1.4941912>
- Nalpanis, P., Hunt, J. C. R., & Barrett, C. F. (1993). Saltating particles over flat beds. *Journal of Fluid Mechanics*, 251, 661–685. <https://doi.org/10.1017/s0022112093003568>
- Nemoto, M., & Nishimura, K. (2004). Numerical simulation of snow saltation and suspension in a turbulent boundary layer. *Journal of Geophysical Research*, 109(D18). <https://doi.org/10.1029/2004jd004657>
- Nishimura, K., & Hunt, J. C. R. (2000). Saltation and incipient suspension above a flat particle bed below a turbulent boundary layer. *Journal of Fluid Mechanics*, 417, 77–102. <https://doi.org/10.1017/s0022112000001014>
- Nishimura, K., & Nemoto, M. (2005). Blowing snow at Mizuho station, Antarctica. *Philosophical Transactions of the Royal Society A: Mathematical, Physical & Engineering Sciences*, 363(1832), 1647–1662. <https://doi.org/10.1098/rsta.2005.1599>
- Nishimura, K., Yokoyama, C., Ito, Y., Nemoto, M., Naaim-Bouvet, F., Bellot, H., & Fujita, K. (2014). Snow particle speeds in drifting snow. *Journal of Geophysical Research: Atmospheres*, 119, 9901–9913. <https://doi.org/10.1002/2014jd021686>
- Okaze, T., Niiya, H., & Nishimura, K. (2018). Development of a large-eddy simulation coupled with Lagrangian snow transport model. *Journal of Wind Engineering and Industrial Aerodynamics*, 183, 35–43. <https://doi.org/10.1016/j.jweia.2018.09.027>
- Owen, P. R. (1964). Saltation of uniform grains in air. *Journal of Fluid Mechanics*, 20(2), 225–242. <https://doi.org/10.1017/s0022112064001173>
- Páhtz, T., Clark, A. H., Valyrosakis, M., & Durán, O. (2020). The physics of sediment transport initiation, cessation, and entrainment across aeolian and fluvial environments. *Reviews of Geophysics*, 58(1), e2019RG000679. <https://doi.org/10.1029/2019rg000679>
- Páhtz, T., Omeradžić, A., Carneiro, M. V., Araújo, N. A. M., & Herrmann, H. J. (2015). Discrete element method simulations of the saturation of aeolian sand transport. *Geophysical Research Letters*, 42, 2063–2070. <https://doi.org/10.1002/2014gl062945>
- Palm, S. P., Kayetha, V., Yang, Y., & Pauly, R. (2017). Blowing snow sublimation and transport over Antarctica from 11 years of CALIPSO observations. *The Cryosphere*, 11(6), 2555–2569. <https://doi.org/10.5194/tc-11-2555-2017>
- Paterna, E., Crivelli, P., & Lehning, M. (2016). Decoupling of mass flux and turbulent wind fluctuations in drifting snow. *Geophysical Research Letters*, 43, 4441–4447. <https://doi.org/10.1029/2016gl068171>
- Paterna, E., Crivelli, P., & Lehning, M. (2017). Wind tunnel observations of weak and strong snow saltation dynamics. *Journal of Geophysical Research*, 122, 1589–1604. <https://doi.org/10.1002/2016jf004111>
- Pomeroy, J. W., & Gray, D. M. (1990). Saltation of snow. *Water Resources Research*, 26(7), 1583–1594. <https://doi.org/10.1029/wr026i007p01583>
- Rice, M. A., Willetts, B. B., & McEwan, I. K. (1995). An experimental study of multiple grain-size ejecta produced by collisions of saltating grains with a flat bed. *Sedimentology*, 42(4), 695–706. <https://doi.org/10.1111/j.1365-3091.1995.tb00401.x>

- Rice, M. A., Willetts, B. B., & McEwan, I. K. (1996). Observations of collisions of saltating grains with a granular bed from high-speed cine-film. *Sedimentology*, 43(1), 21–31. <https://doi.org/10.1111/j.1365-3091.1996.tb01456.x>
- Schiller, L., & Nauman, A. Z. (1933). Über die grundlegenden Berechnungen bei der SchwerSraftaufbereitung. *Zeitschrift des Vereines Deutscher Ingenieure*, 77(12), 318–320.
- Schmidt, D. S., Schmidt, R. A., & Dent, J. D. (1998). Electrostatic force on saltating sand. *Journal of Geophysical Research: Atmospheres*, 103(D8), 8997–9001. <https://doi.org/10.1029/98jd00278>
- Schmidt, R. A. (1980). Threshold wind-speeds and elastic impact in snow transport. *Journal of Glaciology*, 26(94), 453–467. <https://doi.org/10.1017/s002214300010972>
- Shao, Y., & Li, A. (1999). Numerical modelling of saltation in the atmospheric surface layer. *Boundary-Layer Meteorology*, 91(2), 199–225. <https://doi.org/10.1023/a:1001816013475>
- Shao, Y., & Lu, H. (2000). A simple expression for wind erosion threshold friction velocity. *Journal of Geophysical Research*, 105(D17), 22437–22443. <https://doi.org/10.1029/2000jd900304>
- Shao, Y., Raupach, M. R., & Findlater, P. A. (1993). Effect of saltation bombardment on the entrainment of dust by wind. *Journal of Geophysical Research*, 98, 12719–12726. <https://doi.org/10.1029/93jd00396>
- Sharma, V., Comola, F., & Lehning, M. (2018). On the suitability of the Thorpe–Mason model for calculating sublimation of saltating snow. *The Cryosphere*, 12(11), 3499–3509. <https://doi.org/10.5194/tc-12-3499-2018>
- Sharma, V., Parlange, M. B., & Calaf, M. (2017). Perturbations to the spatial and temporal characteristics of the diurnally-varying atmospheric boundary layer due to an extensive wind farm. *Boundary-Layer Meteorology*, 162(2), 255–282. <https://doi.org/10.1007/s10546-016-0195-0>
- Sigmund, A., Dujardin, J., Comola, F., Sharma, V., Huwald, H., Melo, D. B., & Lehning, M. (2021). Evidence of strong flux underestimation by bulk parametrizations during drifting and blowing snowboundary-layer meteorology.
- Sørensen, M. (1991). An analytic model of wind-blown sand transport. In O. E. Barndorff-Nielsen, & B. B. Willetts (Eds.), *Aeolian grain transport 1* (pp. 67–81). Springer Vienna.
- Sørensen, M. (2004). On the rate of aeolian sand transport. *Geomorphology*, 59(1), 53–62.
- Tagliavini, G., McCrorqudale, M., Westbrook, C., Corso, P., Krol, Q., & Holzner, M. (2021). Drag coefficient prediction of complex-shaped snow particles falling in air beyond the Stokes regime. *International Journal of Multiphase Flow*, 140, 103652. <https://doi.org/10.1016/j.ijmultiphaseflow.2021.103652>
- Ungar, J. E., & Haff, P. K. (1987). Steady state saltation in air. *Sedimentology*, 34(2), 289–299. <https://doi.org/10.1111/j.1365-3091.1987.tb00778.x>
- Van Wessem, J. M., van de Berg, W. J., Noël, B. P. Y., van Meijgaard, E., Amory, C., Birnbaum, G., et al. (2018). Modelling the climate and surface mass balance of polar ice sheets using RACMO2 – Part 2: Antarctica (1979–2016). *The Cryosphere*, 12(4), 1479–1498. <https://doi.org/10.5194/tc-12-1479-2018>
- Vionnet, V., Martin, E., Masson, V., Guyomarc'h, G., Naaim-Bouvet, F., Prokop, A., et al. (2014). Simulation of wind-induced snow transport and sublimation in alpine terrain using a fully coupled snowpack/atmosphere model. *The Cryosphere*, 8(2), 395–415. <https://doi.org/10.5194/tc-8-395-2014>
- Vionnet, V., Martin, E., Masson, V., Lac, C., Naaim Bouvet, F., & Guyomarc'h, G. (2017). High-Resolution Large Eddy Simulation of Snow Accumulation in Alpine Terrain. *Journal of Geophysical Research*, 122, 11005–11021. <https://doi.org/10.1002/2017jd026947>
- Walden, V. P., Warren, S. G., & Tuttle, E. (2003). Atmospheric ice crystals over the antarctic plateau in winter. *Journal of Applied Meteorology and Climatology*, 42(10), 1391–1405. [https://doi.org/10.1175/1520-0450\(2003\)042<1391:aicota>2.0.co;2](https://doi.org/10.1175/1520-0450(2003)042<1391:aicota>2.0.co;2)
- Walter, B., Horender, S., Voegeli, C., & Lehning, M. (2014). Experimental assessment of Owen's second hypothesis on surface shear stress induced by a fluid during sediment saltation. *Geophysical Research Letters*, 41, 6298–6305. <https://doi.org/10.1002/2014gl061069>
- Wang, D., Wang, Y., Yang, B., Zhang, W., & Lancaster, N. (2008). Statistical analysis of sand grain/bed collision process recorded by high-speed digital camera. *Sedimentology*, 55(2), 461–470. <https://doi.org/10.1111/j.1365-3091.2007.00909.x>
- Wang, Z., Huang, N., & Pähzt, T. (2019). The effect of turbulence on drifting snow sublimation. *Geophysical Research Letters*, 46, 11568–11575. <https://doi.org/10.1029/2019gl083636>
- Woods, C. P., Stoelinga, M. T., & Locatelli, J. D. (2008). Size spectra of snow particles measured in wintertime precipitation in the Pacific Northwest. *Journal of the Atmospheric Sciences*, 65(1), 189–205. <https://doi.org/10.1175/2007jas2243.1>
- Xing, M., & He, C. (2013). 3D ejection behavior of different sized particles in the grain-bed collision process. *Geomorphology*, 187, 94–100. <https://doi.org/10.1016/j.geomorph.2013.01.002>